CALPHAD: Computer Coupling of Phase Diagrams and Thermochemistry 41 (2013) 89–107

Contents lists available at SciVerse ScienceDirect

CALPHAD: Computer Coupling of Phase Diagrams and Thermochemistry

journal homepage: www.elsevier.com/locate/calphad

Thermodynamic calculation of the Mg–Mn–Zn and Mg–Mn–Ce systems and re-optimization of their constitutive binaries

P. Ghosh, M. Medraj *

Department of Mechanical Engineering, Concordia University, 1455 De Maisonneuve Blvd. West, Montreal, QC, Canada H3G 1M8

ARTICLE INFO

Article history:
Received 8 August 2012
Received in revised form
25 January 2013
Accepted 25 January 2013
Available online 16 February 2013

Keywords:
Mg–Mn–Zn ternary system
Mg–Mn–Ce ternary system
Thermodynamic modeling
Modified quasi-chemical model

ABSTRACT

The Mg–Mn-Ce and Mg–Mn–Zn ternary systems are modeled using the CALPHAD approach. Each constituent binary is critically reviewed in light of available experimental information. Consequently, binaries are re-optimized or directly adopted from the literature. All the binary liquids in the present optimization are modeled by the modified quasi-chemical model (MQM) while the random mixing model is used to describe the terminal solid solutions. The sub-lattice model is applied to the compounds with well-defined solubility range in contrast to the stoichiometric phases which are described as line compounds. Binaries are then extrapolated to form the ternaries without adding any ternary parameters. Very little experimental data is available on these two systems. Nonetheless, the present optimization reproduces most of experimental findings on these binaries as well as ternary systems with reasonable accuracy. Incorporation of future experimental data, as and when available, will refine the present optimization.

1. Introduction

The present study deals with thermodynamic modeling of the Mg–Mn–Zn and Mg–Mn–Ce systems which are two important Mg-alloys ternary systems. The five constituent binaries are critically evaluated based on the available literature data. This section will briefly summarize the literature findings on these systems and subsequently explain the need for re-optimization of few of the constituent binaries.

The latest journal article published on thermodynamic modeling of the Mn–Zn system used Bragg–Williams model [1]. This system will be re-optimized using the modified quasi-chemical model (MQM). The MQM is considered more physically sound than other models such as the associate solution model [2]. In addition, the earlier optimization of the Mn–Zn system [1] only considered phases present above 400 °C and did not include all available literature data. In order to be consistent with the other binaries as well as to achieve closer representation of the experimental results, the Mn–Zn system is re-optimized in the current study. In addition, the present re-optimization takes into account the reported solubility ranges for the compounds which were otherwise not considered in an earlier unpublished work [3].

In case of the Mg–Mn system, contradiction exists in the calculated consolute temperature of the liquid miscibility gap as published by different investigators [4–7]. Kang et al. [4] calculated a much lower value than that of Gröbner et al. [5] and Khan and Medraj [7]. Their respective values could not be verified due to the lack of any experimental data in the literature. The above issue is addressed in the present study and subsequently the Mg–Mn system is re-optimized. Care was taken to improve thermodynamic description over the previous assessments.

In case of the Mg–Ce binary system, the model parameters are mostly taken from the work of Kang et al. [4], except for the incorporation of some minor but important changes. For example, the value for Ce_fcc→Ce_hcp transformation as used by [4] results in an artificial stabilization of hcp_Mg phase in the calculated ternary liquidus surface of the Mg–Mn–Ce system. Besides, the present work critically reviewed the work of Zhang et al. [8] and pointed out the anomaly observed. All these concerns are discussed in detail in Section 2.3. Incorporation of these changes also forced slight modification of the thermodynamic description of this system from that of Kang et al. [4].

The Mn–Ce system was thermodynamically modeled by Kang et al. [4] and Tang et al. [9]. Kang et al. [4] used the MQM to describe the liquid phase but did not take into account the experimentally reported solubility of Mn in Ce. Although Tang et al. [9] did take into account the solubility, they described the liquid phase by random mixing model. Very recently, Kim and Jung [10] re-optimized the system using the MQM for the liquid phase and simultaneously took into account the solubility of Mn

* Corresponding author. Tel.: +1 5148482424; fax: +1 5148483175.
E-mail addresses: mmedraj@encs.concordia.ca, mmedraj@me.concordia.ca (M. Medraj).

0364-5916/$ - see front matter © 2013 Elsevier Ltd. All rights reserved.
http://dx.doi.org/10.1016/j.calphad.2013.01.008

in Ce. They also reported some solubility of Ce in β-Mn and the corresponding reaction β(Mn)—α(Mn)+L was estimated at ~626 °C. Unfortunately, this could not be found in the said reference (ref. no. 26 in Ref. [10]) or any other published literature. In the present study, the liquid phase is re-optimized using the MQM and α-Mn is described by B–W model which was otherwise considered as pure elements in Ref. [10]. These are done in order to be consistent with rest of the binaries. In addition, all the available experimental data are also incorporated. A brief discussion of the literature data on this system is presented in Section 2.4.

In the present study, the Mg–Zn system is directly adopted from the authors' previous work [11] on the Mg–Zn–Sn ternary. The ternary showed good agreement with the experimental findings. Thus, it was worthwhile to use the same thermodynamic description of the Mg–Zn system to construct another ternary, such as Mg–Mn–Zn to verify its applicability. This was successful without even modifying a single parameter. The Mg–Zn phase diagram is shown in Fig. 1 along with experimental data taken from the literature [12–19]. However, careful observations of the assessed diagram have revealed slight modifications of invariant temperatures of the following reactions: $L \leftrightarrow Mg_{51}Zn_{20} + Mg_{12}Zn_{13}$ and $L + Mg\_hcp \leftrightarrow Mg_{51}Zn_{20}$; which are actually at 343 °C. These temperatures were earlier mentioned at 342 °C and 341 °C, respectively. Please note that, nothing has been modified in the thermodynamic description of this system and the changes have come purely from a more accurate visual inspection of the calculated Mg–Zn phase diagram.

In addition, terminal binary solid solutions are given special attention in this work. For example, solid solutions of elements with similar crystal structure in a binary system are modeled using one single Gibbs energy function. This is because it is assumed that pure elements with the same crystal structure should have identical interaction parameters [20] when they form terminal solid solutions having the same crystal structures, due to the random substitutional arrangements of these atoms. This is the reason why Mg_hcp and Zn_hcp terminal solid solutions in the Mg–Zn system are modeled using single Gibbs energy function. Same is followed for δ-Mn and δ-Ce as well as for γ-Mn and γ-Ce phases in the Mn–Ce binary system.

The changes in the constituent binaries necessitate the re-calculation of the ternaries. This is done by extrapolating the constituent binaries. Furthermore, the optimized binaries as well as the ternaries are critically compared with the experimental data from the literature and with the previous assessments.

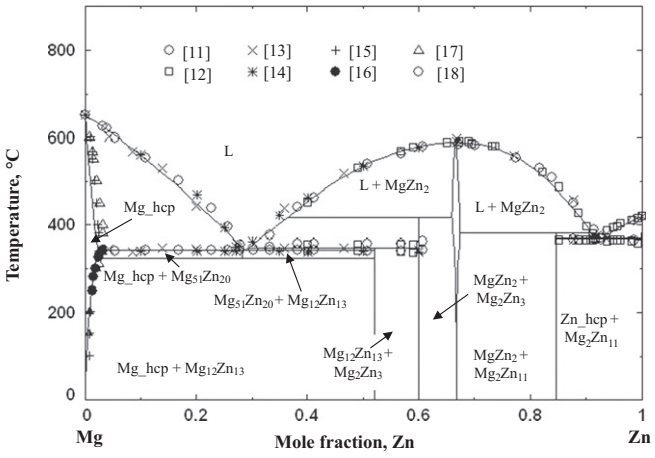

Fig. 1. The Mg–Zn phase diagram from [11].

2. Critical evaluation of the literature data

2.1. Mn–Zn system

Numerous researchers [21–53] have investigated the Mn–Zn system experimentally in order to establish the phase equilibria and obtain the thermodynamic properties of the system. However, many of these experimental results are contradictory. Okamoto and Tanner [54] rigorously reviewed and summarized these earlier experimental works [21–53] on the phase equilibria, thermodynamic properties and the crystal structures of different phases in the Mn–Zn system. Liquid, five terminal solid solutions (α-Mn, β-Mn, γ-Mn, δ-Mn and Zn_hcp) and one intermediate solid solution are reported in the literature. All the Mn terminal solid solutions show appreciable solubility of Zn, except α-Mn which only exhibits 1.7 at% Zn as determined by X-ray diffraction [32,54]. On the contrary, the reported solubility of Mn in Zn_hcp is very small (~0.5 at%). The intermediate solid solution (denoted as 'H' and 'ε' phase in the current and [54] works, respectively) is a controversial phase field. The phase field show a wide composition range (42–88 at% Zn) with the possible presence of three regions. However, the presence of these regions has not been conclusively validated in the published literature. In addition to the solution phases, numerous intermediate compounds are reported as well. Most of these compounds have composition range close to 5–7 at% Zn. Okamoto and Tanner [54] also assessed the Mn–Zn phase diagram, based primarily on the phase equilibria data of Wachtel and Tsiuplakis [47] for the composition range from 60 at% to 100 at% Zn, on Romer and Wachtel [51] for 0–60 at% Zn and above 400 °C and on Nakagawa and Hori [39] for 30–70 at% Zn and below 400 °C.

Miettinen [1] modeled the Mn–Zn system using the experimental data recommended by Okamoto and Tanner [54]. Miettinen [1] used random mixing model for the binary liquid phase and optimized the system above 400 °C. He thus omitted the following phases: ά-$MnZn_3$, γ-Mn_5Zn_8, β_1-MnZn, ζ-$MnZn_{13}$. The only stoichiometric phase considered by him was δ-$MnZn_9$ but he did not incorporate the reported solubility range. Also, the eutectic reaction at the Zn rich side was mentioned as $L \leftrightarrow$ δ-$MnZn_9$ + Zn_hcp instead of $L \leftrightarrow$ ζ-$MnZn_{13}$ + Zn_hcp as suggested in the literature [21–25,28–29,47]. He did not incorporate solubility of Mn in Zn_hcp and instead considered it as zero. In addition, near the Mn-rich part of the phase diagram, his optimization failed to achieve good agreement with the experimental data of Romer and Wachtel [51] who observed wider two solid phase regions of α-Mn (CBCC) and β-Mn (CUB). Recently, Khan [3] in his dissertation used the MQM to describe the liquid phase and significantly improved the thermodynamic description of the system over that of Miettinen [1]. Khan [3] modeled the system starting from room temperature and thus took into account the phases which were otherwise neglected by Miettinen [1]. He modeled γ(Mn_5Zn_8) and H phase using sub-lattice model in order to incorporate the reported solubility ranges and obtained good agreement. However, all the other compounds were described as stoichiometric phases in his work. In the present study, the Mn–Zn system has been further improved by taking into account the solubility ranges reported for the intermediate compounds, which were not taken into consideration by Khan [3].

2.2. Mg–Mn system

A wide miscibility gap exists in the liquid phase of the Mg–Mn system. Experimental data on this system are limited and are inconsistent among one-another. Hashemi and Clark [55] reviewed these data. Very limited solubility of Mn in Mg and negligible solubility of Mg in Mn are observed. No intermetallic

compound is reported in the system. Recently, Gröbner et al. [5] investigated the monotectic reactions in this system by DTA technique using a sealed Ta-crucible and refined the previous results.

Gröbner et al. [5] also revised the previous thermodynamic description of Tibbals [6] based on their new experimental data. They optimized the Mg–Mn liquid phase using random solution model and obtained good fit with the experimental data [5,56]. Recently, Kang et al. [4] and Khan and Medraj [7] re-optimized the system using the MQM for the liquid phase. Kang et al. [4] reported a consolute temperature of the liquid miscibility gap at 1902 °C while Gröbner et al. [5] and Khan and Medraj [7] calculated much higher consolute temperature; 3202 °C and 3415 °C, respectively. In support of their lower consolute temperature, Kang et al. [4] cited Antion [57] argument who questioned the existence of very high consolute temperatures of the binary miscibility gap based on the experimental observation of the consolute temperature of the ternary Mg–Mn–Y system. On the contrary, Khan and Medraj [7] showed that their calculated consolute temperature (3415 °C) is close to the estimated value (~2783 °C) according to Predel's derivation [58] which is as follows: $T_c \approx 2\Delta H_m/R + 2\Delta s_m^x$; where, H_m is molar enthalpy of mixing, S_m^x is excess entropy of mixing. They also pointed out that the percentage deviation between the calculated and the estimated value in this case is within the percentage deviation of other similar systems such as Al–In, Al–Pb, Bi–Zn and Cd–Ga. Khan and Medraj [7] argued that it is more reasonable to evaluate the system on the basis of such thermodynamic considerations rather than the use of single experimental information in a specific higher order system to validate the reliability of the calculation in a lower order system as performed by Kang et al. [4]. Their argument was further substantiated by the fact that there is no other experimental information available on any other ternary systems involving Mg–Mn as a constituent binary, except the results of Antion [57] to support the conclusion made by Kang et al. [4].

2.3. Mg–Ce system

This system has been extensively reviewed by Nayeb-Hashemi and Clark [59] and thermodynamically optimized by Cacciamani et al. [60]. Later on Kang et al. [4] optimized this system using the MQM for the liquid phase. Zhang et al. [61] studied experimentally the intermetallic compounds in this system using laboratory prepared samples. They observed a shift in the position of $Mg_{12}Ce$ from its theoretical value of 7.69 at% Ce. The measurement showed a value of 8.22 at% Ce at the left boundary, and 8.47 at% Ce at the right. They have therefore re-designated $Mg_{12}Ce$ as $Mg_{11}Ce$, with composition range of $Mg_{(11.17-10.8)}Ce$ at room temperature. They argued that probably $Mg_{11}Ce$ is a defect structure of $Mg_{12}Ce$ with vacancies substituting Mg sites [61]. They also refuted the existence of $Mg_{10.3}Ce$ phase (same as $Mg_{17}Ce_2$) being very close to 10.8 at% Ce, the right boundary of $Mg_{11}Ce$. However, in a subsequent publication [8] on the thermodynamic description of the same system, the same group of authors used $Mg_{12}Ce$ instead of $Mg_{11}Ce$ and also considered the existence of $Mg_{17}Ce_2$ phase. In this case, Zhang et al. [8] only changed the enthalpy of formation values of $Mg_{12}Ce$, taking all the other parameters from Kang et al. [4]. However, by doing so, they could reduce the eutectic temperature at the Mg-side from 601 °C to 593 °C but disturbed the other invariant reaction temperatures. Cacciamani et al. [60] and Kang et al. [4] used 50,000 J/mol and 5230 J/mol for the Gibbs energy of the hypothetical phase transformation from pure stable Ce_fcc to unstable Ce_hcp, respectively and obtained reasonably good fit with the experimental phase diagram and thermodynamics properties. Kang et al. [4] reduced this value to accommodate the observed large solubility of Ce in Y_hcp. However, experimental information is limited on Ce–Y system and very few data points are available only with significant scatter. Wang et al. [62] suggested a value of 8500 J/mole for this transformation (Ce_fcc → Ce_hcp) from their first principle calculation at 0 K. Meng et al. [63] adopted this value and successfully reproduced Ce–Y system.

2.4. Mn–Ce system

The first investigation on the Mn–Ce system was carried out by Rolla and Iandelli [64,65] who reported two thermal arrests at 612 °C and 998 °C. The second thermal arrest was interpreted as a monotectic temperature associated with a narrow miscibility gap between 68 at% and 82 at% Mn. However, the existence of the miscibility gap was not confirmed by Mirgalovskaya and Strel'nikova [66] neither later on by Tang et al. [9]. Thamer [67] investigated the phase relationships in the Ce-rich region (below 20 at% Mn) by differential thermal analysis (DTA), metallography and X-ray diffraction technique using high purities Ce (99.8% pure) and Mn (99.96% pure) starting materials. He [67] reported the eutectic reaction to occur at 16.1 ± 0.5 at% Mn and 622 °C. Perkins et al. [68] reported this temperature to be at 618 ± 3 °C and at 14 at% Mn. Iandelli [65] placed this eutectic reaction at a temperature of 612 °C and 15.1 at% Mn liquid composition while Mirgalovskaya and Strel'nikova [66] determined it at 12 at% Mn liquid composition and 635 °C temperature. Thamer [67] reported two catatectic reactions; (i) δ-Ce ↔ γ-Ce + Liquid at 5 ± 1 at% Mn and 638 °C temperature and (ii) β-Mn ↔ α-Mn + Liquid at 625 °C. Thamer [67] also determined the solubilities of Mn in δ-Ce and γ-Ce and reported values of 5 at% and 2 at% Mn at 638 °C, respectively, and indicated that the solubility of Mn in γ-Ce drops to less than 1 at% at 600 °C. By examining lattice parameters, Iandelli [65] found that α-Mn dissolves negligible amount of Ce at room temperature. Tang et al. [9] in their work on thermodynamic assessment of the Mn–Ce system quoted the solubility of Ce in (β-Mn) as 1.8 at% Ce (reference [7] of [9], which was listed as 'under review'). Unfortunately, the present authors could not find this paper in the published literature. Another published article [69] by the same group of authors on the same topic also did not report any such finding. This system does not have intermediate compounds.

Kang et al. [4], Tang et al. [9] and Kim and Jung [10] assessed the Mn–Ce system thermodynamically. While Kang et al. [4] and Kim and Jung [10] used the MQM for the liquid phase, Tang et al. [9] used simple random mixing model. However, surprisingly Kang et al. [4] assumed negligible solubility of Mn in both γ-Ce and δ-Ce. Also their calculated transition temperature from δ-Ce ↔ γ-Ce was much higher (~724 °C) than ~638 °C, the experimental value reported in the literatures [9,67]. Kim and Jung [10] considered the solubility of Mn in Ce and at the same time reported some solubility of Ce in β-Mn. Unfortunately, the later one could not be found in the mentioned reference (ref. no. 26 in Ref. [10]) or any other published literature. In the present study, the liquid phase is re-optimized using the MQM and α-Mn is described by B–W model which was otherwise considered as pure elements in Ref. [10]. These are done in order to be consistent with rest of the binaries. All the other available experimental data are also incorporated.

2.5. Mg–Mn–Ce ternary system

There are very few experimental data on the Mg–Mn–Ce system. Mikheeva [70] measured an isothermal section at 530 °C in the Mg-rich region. No ternary phases in equilibrium with Mg_hcp were observed. Petrov et al. [71] reported two

vertical sections (0.3 wt% and 1.6 wt% Ce) in the Mg-rich region constructed by thermal and microscopic methods. A columnar structure in Mg-rich alloy was reported by Chukhrov and Khrisanova [72] which is believed to be the results of a ternary eutectic reaction ($L \rightarrow Mg\_hcp + \alpha\text{-}Mn + CeMg_{12}$) as suggested by Kang et al. [73]. Recently, Zhang et al. [8] determined three vertical sections at 0.6 wt%, 1.8 wt% and 2.5 wt% Mn by cooling curve analysis (CCA) and differential scanning calorimetry (DSC). No other experimental data could be found in the open literature.

Kang et al. [4,73] performed thermodynamic modeling on this system by extrapolating the constituent binaries. Later on, based on the experimental findings [61,74], Zhang et al. [8] modified the free energy of the $Mg_{12}Ce$ intermetallic compound but kept all the other parameters of Kang et al. [4,73] the same. All the solid solution phases were modeled using compound energy formalism (CEF) in their work [4,8]. They [4,8] also assumed no solubility of Mn in δ-Ce and γ-Ce which was contrary to the experimental data of Thamer [67] who measured 5 at% and 2 at% solubility of Mn at 638 °C in δ-Ce and γ-Ce, respectively. In the present study all the terminal solid solutions are described using Bragg–Williams Model taking into consideration the solubility of Mn in δ-Ce and γ-Ce according to the reported experimental data in the literature. Also, δ-Ce and δ-Mn are modeled using a single Gibbs energy function considering their identical crystal structure. Similar approach has been taken for γ-Ce and γ-Mn. Apart from these, Kang et al. [4,73] placed the consolute temperature of the Mg–Mn liquid at much lower temperature than the current work.

2.6. Mg–Mn–Zn ternary system

Only two experimental measurements, one by Joel and Schneider [75] and the other by Bumazhnov [76], on the Mg–Mn–Zn phase equilibria have been found in the literature. Raynor [77] and later on Ohno and Schmid-Fetzer [78] reviewed these works and only the key aspects are summarized here. Bumazhnov [76] calculated the solubility of Mn and Zn in the Mg solid solution by microstructural analyses and XRD measurements. He observed a significant increase in Mn solubility in the Mg solid solution with decreasing amount of Zn. Joel and Schneider [75] studied the ternary phase equilibrium in the Mg-rich region which was found only qualitatively consistent with the work of Bumazhnov [76] by Ohno and Schmid-Fetzer [78]. Ohno and Schmid-Fetzer [78] also presented a thermodynamic description of the Mg–Mn–Zn system which unfortunately does not agree with none of the two available experimental data [75,76]. Ohno and Schmid-Fetzer [78] disputed the results of Bumazhnov's [76] experiment on the ground that the 30 days annealing period and the subsequent isothermal holding for 7 days at different temperatures may not be sufficient for the required solid state equilibrium in the Mg-rich corner of the Mg–Mn–Zn system. Ohno and Schmid-Fetzer [78] also criticized the technique of microstructural observation in detecting the solubility limit of Mn in Mg solid solution in the Mg–Mn–Zn system for its inherent difficulties. Ohno and Schmid-Fetzer [78] termed the ternary invariant reaction $L + \alpha\text{-}Mn \leftrightarrow Mg\_hcp + Mg_{51}Zn_{20}$ depicted by Joel and Schneider [75] as unreasonable and corrected it to $L + Mg\_hcp \leftrightarrow \alpha\text{-}Mn + Mg_{51}Zn_{20}$ on the basis of the well-established thermodynamic description of the Mg–Zn system. Ohno and Schmid-Fetzer [78] calculated Zn composition dependence of the incipient melting temperature of Mg-0.2 wt% Mn–Zn alloy and compared it with the experimental data of [79]. They achieved better consistency near the low Zn concentration but very poor consistency as Zn concentration increases.

3. Thermodynamic models

3.1. Pure elements

The Gibbs energy of pure element i (i=Mg, Mn, Ce and Zn) in a certain phase φ is described as a function of temperature by the following equation:

$$^{0}G_i^{\varphi}(T) = a + bT + cT\ln T + dT^2 + eT^3 + fT^{-1} + gT^7 + hT^{-9} \quad (1)$$

where, $^{0}G_i^{\varphi}(T)$ is the Gibbs energy at standard state and T is the absolute temperature. The values of the coefficients a to h are taken from the SGTE (Scientific Group Thermodata Europe) compilation by Dinsdale [80].

3.2. Liquid phase

The liquid phase is modeled in this work using the MQM where the pair approximation is utilized to describe the short range ordering (SRO). It is observed that the alloy systems which show a strong compound forming tendency in the solid state (i.e., Mg–Zn, Mg–Ce etc.) display a pronounced minimum in the enthalpy of mixing of the liquid phase and this is caused by the existence of short-range ordering [81]. The Bragg–Williams random-mixing model needs too many parameters to describe binary solutions having short-range ordering and thus not considered very effective. The "associate" or "molecular" model [82] was also proposed to deal with the short-range ordering. However this model assumes that some molecules occupy certain atomic sites which are not physically sound. Another important weakness of the "associate" model is its inability to predict the correct thermodynamic properties of ternary solutions when the binary sub-systems exhibit short-range ordering [83]. A detailed description of the MQM can be found elsewhere [2,84].

3.3. Terminal solid solutions

Random solution model is used to describe the disordered terminal solid solution phases. The excess Gibbs energy is expressed using Redlich–Kister polynomial [85] according to the following equation.

$$G = x_i^0 G_i^{\varphi} + x_j^0 G_j^{\varphi} + RT[x_i \ln x_i + x_j \ln x_j] + {}^{ex}G_{\varphi} \quad (2)$$

where, $^{ex}G^{\varphi}$ is the excess Gibbs energy function expressed as

$$^{ex}G^{\varphi} = X_A X_B [{}^{0}L_{A,B}^{\varphi} + (X_A - X_B)^{1}L_{A,B}^{\varphi} + (X_A - X_B)^{22}L_{A,B}^{\varphi}].$$

Each of the L term may be temperature dependent according to

$$^{n}L_{A,B}^{\varphi} = a + b(T).$$

The parameters a and b are obtained by optimization using experimental results of phase equilibria and thermodynamic data.

3.4. Intermediate compounds

All the intermediate compounds in the Mg–Ce system are considered stoichiometric. The Gibbs energy for a stoichiometric compounds is described by the following equation:

$$G^{\varphi} = x_i^0 G_i^{\varphi 1} + x_j^0 G_j^{\varphi 2} + \Delta G^f \quad (3)$$

where, φ denotes the phase of interest, x_i and x_j are the mole fraction of components i and j and $G_i^{\varphi 1}$ and $G_j^{\varphi 2}$ represent the Gibbs energy in their standard state and $\delta G^f = a + bT$ is the Gibbs energy of formation per mole of atoms of the stoichiometric

Table 1
The stable phases and the model used to describe them in the Mg–Mn–(Ce, Zn) system.

Type	Phase	System	Model used
Terminal solid solution	Hcp	Mg–Mn, Mg–Zn, Mn–Zn, Mg–Ce	B–W
	δ_bcc	Mg–Mn, Mn–Ce, Mn–Zn, Mg–Ce	
	γ_fcc	Mg–Mn, Mn–Ce, Mn–Zn, Mg–Ce	
	α-Mn	Mg–Mn, Mn–Ce, Mn–Zn	
	β-Mn	Mg–Mn, Mn–Ce, Mn–Zn	
	dhcp_Ce	Mn–Ce, Mg–Ce	Pure element
Intermediate phase	$\delta_1(MnZn_9)$	Mn–Zn	Sub-lattice
	$\delta(MnZn_9)$		Sub-lattice
	$\acute{\alpha}$-$MnZn_3$		Sub-lattice
	H*		MQM
	γ-Mn_5Zn_8		Sub-lattice
	$MgZn_2$	Mg–Zn	Sub-lattice
Compounds	$Mg_{12}Ce$	Mg–Ce	Stoichiometry
	$Mg_{17}Ce_2$		
	$Mg_{41}Ce_5$		
	Mg_3Ce		
	Mg_2Ce		
	MgCe		
	β_1-MnZn	Mn–Zn	Stoichiometry
	ζ-$MnZn_{13}$		
	Mg_2Zn_{11}	Mg–Zn	Stoichiometry
	Mg_2Zn_3		
	$Mg_{12}Zn_{13}$		
	$Mg_{51}Zn_{20}$		
Liquid	liquid	Mg–Mn, Mg–Zn, Mn–Zn, Mg–Ce, Mn–Ce	MQM

* Designated as 'ε' phase in previous study [54].

compound. The parameters a and b are determined in a similar fashion to that of terminal solid solutions.

Two intermediate phases, $\zeta(MnZn_{13})$ and $\beta_1(MnZn)$ in the Mn–Zn system are modeled as stoichiometric phases. The other compounds in this system are described using the compound energy formalism (CEF) [86,87]. For example, the $MgZn_2$ (Laves) phase in the Mg–Zn system [11] is modeled using two sublattices; (Mg, Zn) and (Mg, Zn)$_2$. This model of two sublattices covers the whole composition range and therefore the homogeneity range of $MgZn_2$ (~66–67.1 at % Zn) could be successfully reproduced. Similarly, in the case of Mn_5Zn_8 in the Mn–Zn system; two sublattices have been considered with only Zn in the second sublattice with eight sites and mixing both Mn and Zn atoms on the first sublattice with five sites. The Gibbs energy per formula unit is given by:

$$\Delta G^{Mn_5Zn_8} = y_{Zn}\,{}^0G_{Zn:\,Zn} + y_{Mn}\,{}^0G_{Mn:\,Zn} + 5RT\left[y_{Zn}\ln y_{Zn} + y_{Mn}\ln y_{Mn}\right] + y_{Zn}\times y_{Mn}\,{}^0L_{Mn,Zn} \quad (4)$$

where, y_{Zn} and y_{Mn} are the site fractions of Zn and Mn on the first sublattice, respectively. Gibbs energy of formation of the end members ${}^0G_{Zn:Zn}$ and ${}^0G_{Zn:Mn}$ and the L terms are optimized to fit the experimental data.

3.5. Intermediate solid solutions

In addition to the liquid phases, the 'H' phase (intermediate solid solution) in the Mn–Zn system is modeled using the MQM to reproduce its large solubility range.

There are no compounds in the Mg–Mn and Mn–Ce systems. Also no ternary compounds are reported in both the ternaries of interest (Mg–Mn–Ce and Mg–Mn–Zn). In the present study, the constituent binaries are extrapolated according to the Kohler extrapolation method [88] to construct the ternaries without addition of any ternary parameters.

The terminology and the models used in this work in describing the Gibbs energy of all the stable phases in the Mg–Mn–(Ce, Zn) system are listed in Table 1 and all the optimized model parameters of different phases are summarized in Tables 2–6.

Table 2
Gibbs free energy of stable and hypothetical pure elements.

Phase	Pure element	Gibbs energy (J/mol)	Nature of the phase	Refs.
hcp	Mg	${}^0G_{Mg}^{hcp}$	Stable	[79]
	Ce	${}^0G_{Mg}^{hcp} = {}^0G_{Ce}^{fcc} + 8000$	Hypothetical	This work
	Mn	${}^0G_{Mn}^{hcp} = {}^0G_{Mn}^{cbcc} + 3700$	Hypothetical	This work
	Zn	${}^0G_{Zn}^{hcp}$	Stable	[79]
γ	Mg	${}^0G_{Mg}^{\gamma} = {}^0G_{Mg}^{hcp} + 3000 - T$	Hypothetical	This work
	Ce	${}^0G_{Ce}^{\gamma}$	Stable	[79]
	Mn	${}^0G_{Mn}^{\gamma}$	Stable	[79]
	Zn	${}^0G_{Zn}^{\gamma} = {}^0G_{Zn}^{hcp} + 2970 - 1.5T$	Hypothetical	This work
δ	Mg	${}^0G_{Mg}^{\delta} = {}^0G_{Mg}^{hcp} + 3000 - 1.9T$	Hypothetical	This work
	Ce	${}^0G_{Ce}^{\delta}$	Stable	[79]
	Mn	${}^0G_{Mn}^{\delta}$	Stable	[79]
	Zn	${}^0G_{Zn}^{\delta} = {}^0G_{Zn}^{hcp} + 2687 - 2T$	Hypothetical	This work
α-Mn	Mg	${}^0G_{Mg}^{\alpha\text{-}Mn} = {}^0G_{Mg}^{hcp} + 4600$	Hypothetical	This work
	Ce	${}^0G_{Ce}^{\alpha\text{-}Mn} = {}^0G_{Ce}^{fcc} + 5000$	Hypothetical	This work
	Mn	${}^0G_{Mn}^{\alpha\text{-}Mn}$	Stable	[79]
	Zn	${}^0G_{Zn}^{\alpha\text{-}Mn} = {}^0G_{Zn}^{hcp} + 3000$	Hypothetical	This work
β-Mn	Mg	${}^0G_{Mg}^{\beta\text{-}Mn} = {}^0G_{Mg}^{hcp} + 4600$	Hypothetical	This work
	Ce	${}^0G_{Ce}^{\beta\text{-}Mn} = {}^0G_{Ce}^{fcc} + 20{,}000 + 5T$	Hypothetical	This work
	Mn	${}^0G_{Mn}^{\beta Mn}$	Stable	[79]
	Zn	${}^0G_{Zn}^{\beta\text{-}Mn} = {}^0G_{Zn}^{hcp} + 3000$	Hypothetical	This work

Table 3
Optimized model parameters for the liquid phase in the Mg–Mn–(Ce, Zn) system.

System	Model parameters		Model used	Refs.
	Coordination Number	Parameters; J/mole		
Mg–Mn	$Z^{Mg}_{Mg,Mn}=4$, $Z^{Mn}_{Mn,Mg}=6$ $Z^{Mg}_{Mg,Mg}=Z^{Mn}_{Mn,Mn}=6$	$\Delta g^{0}=22{,}970.2$ $\Delta g^{10}=-12{,}999.35$	MQM	This work
Mg–Ce	$Z^{Mg}_{Mg,Ce}=2$, $Z^{Ce}_{Ce,Mg}=6$ $Z^{Mg}_{Mg,Mg}=Z^{Ce}_{Ce,Ce}=6$	$\Delta g^{0}=-15{,}914.4+7.44\,T$ $\Delta g^{10}=-9{,}632.4+2.51\,T$ $\Delta g^{01}=-8{,}371.8$	MQM	[4]
Mg–Zn	$Z^{Mg}_{Mg,Zn}=4$, $Z^{Zn}_{Zn,Mg}=6$ $Z^{Mg}_{Mg,Mg}=Z^{Zn}_{Zn,Zn}=6$	$\Delta g^{0}=-8{,}326.2+3.19\,T$ $\Delta g^{10}=-460.24-3.27\,T$ $\Delta g^{01}=-62.76-3.77\,T$	MQM	[11]
Mn–Ce	$Z^{Mn}_{Mn,Ce}=3$, $Z^{Ce}_{Mn,Ce}=6$ $Z^{Mn}_{Mn,Mn}=Z^{Ce}_{Ce,Ce}=6$	$\Delta g^{0}=5{,}564.72-0.84\,T$ $\Delta g^{10}=-1.046\,T$ $\Delta g^{01}=-1{,}004.16+1.26\,T$	MQM	This work
Mn–Zn	$Z^{Mn}_{Mn,Zn}=6$, $Z^{Zn}_{Zn,Mn}=6$ $Z^{Mn}_{Mn,Mn}=Z^{Zn}_{Zn,Zn}=6$	$\Delta g^{0}=-3{,}249.71+1.38\,T$	MQM	This work

Table 4
Optimized model parameters for the terminal solid solutions in the Mg–Mn–(Ce, Zn) system.

Phase	Components	Parameters (J/mol)	Model used	Refs.
Mg_hcp	Mg–Mn	${}^{0}L^{Mg\_hcp}_{Mg,Mn}=32{,}000$	B–W	This work
Zn_hcp	Mg–Ce	${}^{0}L^{Mg\_hcp}_{Mg,Ce}=-24{,}476.4$	B–W	[4]
	Mg–Zn	${}^{0}L^{Mg,Zn\_hcp}_{Mg,Zn}=-1200+6.5T$	B–W	[11]
	Mn–Zn	${}^{0}L^{Zn\_hcp}_{Mn,Zn}=5000-3T$	B–W	This work
γ-Ce	Ce–Mn	${}^{0}L^{\gamma\text{-}Ce,Mn}_{Ce,Mn}=29{,}000+3.5T$; ${}^{1}L^{\gamma\text{-}Ce,Mn}_{Ce,Mn}=1.9T$	B–W	This work
γ-Mn	Ce–Mg	${}^{0}L^{\gamma\text{-}Ce}_{Ce,Mg}=-9273.0$	B–W	This work
	Mn–Mg	${}^{0}L^{\gamma\text{-}Mn}_{Mn,Mg}=80{,}000$	B–W	This work
	Mn–Zn	${}^{0}L^{\gamma\text{-}Mn}_{Mn,Zn}=-12{,}900+2.535T$	B–W	This work
δ-Ce	Ce–Mn	${}^{0}L^{\delta\text{-}Ce,Mn}_{Ce,Mn}=31{,}740-5.7T$; ${}^{1}L^{\delta\text{-}Ce,Mn}_{Ce,Mn}=6T$	B–W	This work
δ-Mn	Ce–Mg	${}^{0}L^{\delta\text{-}Ce}_{Ce,Mg}=-15594-9.75T$; ${}^{1}L^{\delta\text{-}Ce}_{Ce,Mg}=-9000$	B–W	This work
	Mn–Mg	${}^{0}L^{\delta\text{-}Mn}_{Mn,Mg}=80{,}000$	B–W	This work
	Mn–Zn	${}^{0}L^{\delta\text{-}Mn}_{Mn,Zn}=-12{,}310+2.1T$; ${}^{1}L^{\delta\text{-}Mn}_{Mn,Zn}=1500-1.0T$	B–W	This work
α-Mn	Mn–Ce	${}^{0}L^{\alpha\text{-}Mn}_{Mn,Ce}=80{,}000$	B–W	This work
	Mn–Mg	${}^{0}L^{\alpha\text{-}Mn}_{Mn,Mg}=80{,}000+50T$	B–W	This work
	Mn–Zn	${}^{0}L^{\alpha\text{-}Mn}_{Mn,Zn}=10{,}000$	B–W	This work
β-Mn	Mn–Ce	${}^{0}L^{\beta\text{-}Mn}_{Mn,Ce}=80{,}000+100T$		
	Mn–Mg	${}^{0}L^{\beta\text{-}Mn}_{Mn,Mg}=80{,}000+50T$	B–W	This work
	Mn–Zn	${}^{0}L^{\beta\text{-}Mn}_{Mn,Zn}=-30{,}877+71.7T$; ${}^{1}L^{\beta\text{-}Mn}_{Mn,Zn}=47{,}000+84.35T$; ${}^{2}L^{\beta\text{-}Mn}_{Mn,Zn}=75{,}730+9.62T$	B–W	This work

4. Thermodynamic optimization

4.1. Mn–Zn binary system

The optimized Mn–Zn phase diagram resulting from the current work is shown in Fig. 2 together with the experimental data of Nakagawa and Hori [39], Romer and Wachtel [51] and Wachtel and Tsiuplakis [47] recommended by Okamoto and Tanner [54]. Unlike the work of Miettinen [1], the current modeling takes into account all the phases present below or above 400 °C. The present model also consideres the solubility ranges reported for δ ($MnZn_9$), δ_1 ($MnZn_9$) and α ($MnZn_3$) which were otherwise considered as stoichiometric compounds by Khan [3]. The γ(Mn_5Zn_8) and H phases are modeled using the sublattice and the MQM, respectively; while ζ($MnZn_{13}$) and β_1(MnZn) compounds are described as stoichiometric phases, similar to that of Khan [3].

In Table 7, the calculated invariant reactions in the Mn–Zn binary system are compared with the experimental data from the literature [21–22,24–25,29,32,39,47,51]. It is seen from this table, that most of the experimentally observed invariant reactions are reasonably reproduced. The liquidus phase boundaries were measured by many investigators and most of them showed good consistency with each other. However, disagreement in various reports and the lack of confirming data were found for solid phases [54]. In the current work the calculated liquidus shows good agreement with the measured data. The maximum solubility of Zn in α-Mn is reported as 1.7 at% by X-ray diffraction study

Table 5
Optimized model parameters for the intermediate solid solutions in Mg–Mn–(Ce, Zn) system

System	Phase	Parameters (J/mol). (J/mol/K)	Model used	Refs.
Mn–Zn	δ_1 ($MnZn_9$)	${}^0G^{Mn_{10}}_{Mn,Mn} = 10G(\alpha\text{-Mn,cbcc\_Mn}) + 50{,}000$ ${}^0G^{Mn_9Zn}_{Mn,Zn} = 9G(\alpha\text{-Mn,cbcc\_Mn}) + G(\text{Zn, hcp\_Zn}) + 50{,}000 + 200T$ ${}^0G^{Zn_{10}}_{Zn,Zn} = 10G(\text{Zn,hcp\_Zn}) + 50{,}000 + 10T$ ${}^0\Delta H^{MnZn_9}_{298.15K} = -17{,}500$; ${}^0\Delta S^{MnZn_9}_{298.15K} = 417.97$ $C_p = C_p(\alpha\text{-Mn, cbcc\_Mn}) + 9C_p(\text{Zn, hcp\_Zn})$ ${}^0L^{MnZn_9}_{Mn,Zn:Mn} = -15{,}000$; ${}^0L^{MnZn_9}_{Mn,Zn:Zn} = -10{,}000 - 15T$ ${}^0L^{MnZn_9}_{Mn:Mn,Zn} = -10{,}000$; ${}^0L^{MnZn_9}_{Zn:Mn,Zn} = -50{,}000$	Sub-lattice	This work
	δ ($MnZn_9$)	${}^0G^{Mn_{10}}_{Mn,Mn} = 10G(\alpha\text{-Mn,cbcc\_Mn}) + 13{,}000 + 130T$ ${}^0G^{Mn_9Zn}_{Mn,Zn} = 9G(\alpha\text{-Mn, cbcc\_Mn}) + G(\text{Zn,hcp\_Zn}) + 10{,}000 + 100T$ ${}^0G^{Zn_{10}}_{Zn,Zn} = 10G(\text{Zn,hcp\_Zn}) + 15{,}000 + 100T$ ${}^0\Delta H^{MnZn_9}_{298.15K} = -17{,}500$; ${}^0\Delta S^{MnZn_9}_{298.15K} = 417.97$ $C_p = C_p(\alpha\text{-Mn, cbcc\_Mn}) + 9C_p(\text{Zn, hcp\_Zn})$ ${}^0L^{MnZn_9}_{Mn,Zn:Mn} = -30{,}000$; ${}^0L^{MnZn_9}_{Mn,Zn:Zn} = -13{,}000 - 100T$ ${}^0L^{MnZn_9}_{Mn:Mn,Zn} = -100{,}000 - 10T$	Sub-lattice	This work
	ά-$MnZn_3$	${}^0G^{Mn_4}_{Mn,Mn} = 4G(\alpha\text{-Mn,cbcc\_Mn}) + 25{,}000 + 20T$ ${}^0G^{Mn_3Zn}_{Mn,Zn} = 3G(\alpha\text{-Mn,cbcc\_Mn}) + G(\text{Zn,hcp\_Zn}) + 14{,}000 + 10T$ ${}^0G^{Zn_4}_{Zn,Zn} = 4G(\text{Zn,hcp\_Zn}) + 20{,}000 + 20T$ ${}^0\Delta H^{MnZn_3}_{298.15\ K} = -15{,}000$; ${}^0\Delta S^{MnZn_3}_{298.15\ K} = 160.25$ $C_p = C_p(\alpha\text{-Mn, cbcc\_Mn}) + 3C_p(\text{Zn, hcp\_Zn})$ ${}^0L^{MnZn_3}_{Mn,Zn:Mn} = 50{,}000 + 100T$; ${}^0L^{MnZn_3}_{Mn,Zn:Zn} = -22{,}000$ ${}^0L^{MnZn_3}_{Mn:Mn,Zn} = -60{,}000 + 35T$; ${}^0L^{MnZn_3}_{Zn:Mn,Zn} = 20{,}000$	Sub-lattice	This work
	H-phase	$\Delta g^0_{Mn,Zn} = -744.3 - 1.975T$ $\Delta g^{10}_{Mn,Zn} = -794.96 + 1.1506T$ $\Delta g^{01}_{Mn,Zn} = -10{,}167.12 + 8.87T$	MQM	This work
	γ-Mn_5Zn_8	${}^0G^{Mn_5Zn_8}_{Mn,Zn} = 5G(\alpha\text{-Mn,cbcc\_Mn}) + 8G(\text{Zn,hcp\_Zn}) + 98{,}491.38 - 56.90T$ ${}^0G^{Zn_{13}}_{Zn,Zn} = 13G(\text{Zn,hcp\_Zn}) + 962.32$ ${}^0L^{Mn_5Zn_8} = -199{,}995.2 + 197.4848T$	Sub-lattice	This work
Mg–Zn	$MgZn_2$ LAVE	${}^0G^{Mg3}_{Mg:Mg} = 3G(\text{Mg,hcp\_A3}) + 43.49 \times 10^3$ ${}^0G^{Zn3}_{Zn:Zn} = 3G(\text{Zn,hcp\_Zn}) + 20 \times 10^3$ ${}^0G^{Mg_2Zn}_{Mg:Zn} = 2G(\text{Mg,hcp\_A3}) + G(\text{Zn,Hcp\_Zn}) + 30 \times 10^3$ ${}^0G^{MgZn_2}_{Mg:Zn} - 55{,}979.23 + 380.999T - 74T\ln T + 0.00085T^2 - 3.333 \times 10^{-6}T^3$ ${}^0\Delta H^{MgZn_2}_{298.15\ K} = -33{,}815$; ${}^0S^{MgZn_2}_{298.15\ K} = 115.005$; $Cp = 74 - 0.0017T + 2 \times 10^{-5}T^2$ ${}^0L^{MgZn_2}_{Mg,Zn:Mg} = {}^0L^{MgZn_2}_{Mg,Zn:Zn} = {}^0L^{MgZn_2}_{Mg:Mg,Zn} = {}^0L^{MgZn_2}_{Zn:Mg,Zn} = 1.0$	Sub-lattice	[11]

of Potter and Huber [32] which is higher than the value calculated by the preset study of 0.38 at%. However, the maximum solubility of Mn in Zn is calculated as 0.38 at% at eutectic temperature, closer to the reported value of 0.58 at% by [28]. The boundary between β-Mn/[β-Mn + α-Mn] was determined at 16 ± 1 at% Zn at 400 °C [32,51] which is very close to the estimated value from this study (14.8 at% Zn). A wide variation of the maximum solubility of Zn in β-Mn was noticed in the literature. The reported values are 48 at% [39], 17.4 at% [32] and 23 at% [51]. The present study calculates a value of 32.3 at% Zn, in between the reported values in the literature. Potter and Huber [32] reported a wider γ-Mn phase field than that of Romer and Wachtel [51]. The present finding also showed a wider field. In addition, it should be pointed out that the possible order-disorder transition of the δ-Mn phase has not been considered in the present modeling as no experimental evidence could be found in the literature. The most

Table 6
Optimized model parameters for the stoichiometric compounds in Mg–Mn–(Ce, Zn) system.

System	Compound	Parameters (J/mol), (J/mol/K)	Model used	Refs.
Mg–Ce	$Mg_{12}Ce$	${}^0\Delta H^{Mg_{12}Ce}_{298.15\ K} = -139{,}880.2$; ${}^0S^{Mg_{12}Ce}_{298.15\ K} = 377.01$ $C_p = 12C_p$(Mg, hcp_A3)$+C_p$(Ce, fcc_Ce)	Stoichiometric	[4]
	$Mg_{17}Ce_2$	${}^0\Delta H^{Mg_{17}Ce_2}_{298.15\ K} = -215{,}906$; ${}^0S^{Mg_{17}Ce_2}_{298.15\ K} = 591.63$ $C_p = 17C_p$(Mg, hcp_A3)$+2C_p$(Ce, fcc_Ce)	Stoichiometric	[4]
	$Mg_{41}Ce_5$	${}^0\Delta H^{Mg_{41}Ce_5}_{298.15\ K} = -576{,}002$; ${}^0S^{Mg_{41}Ce_5}_{298.15\ K} = 1387.78$ $C_p = 41C_p$(Mg, hcp_A3)$+5C_p$(Ce, fcc_Ce)	Stoichiometric	[4]
	Mg_3Ce	${}^0\Delta H^{Mg_3Ce}_{298.15\ K} = -76{,}000$; ${}^0S^{Mg_3Ce}_{298.15\ K} = 140.97$ $C_p = 3C_p$(Mg, hcp_A3)$+C_p$(Ce, fcc_Ce)	Stoichiometric	[4]
	Mg_2Ce	${}^0\Delta H^{Mg_2Ce}_{298.15\ K} = -47{,}449$; ${}^0S^{Mg_2Ce}_{298.15\ K} = 124.5$ $C_p = 2C_p$(Mg, hcp_A3)$+C_p$(Ce, fcc_Ce)	Stoichiometric	[4]
	MgCe	${}^0\Delta H^{MgCe}_{298.15\ K} = -28{,}600$; ${}^0S^{MgCe}_{298.15\ K} = 97.08$ $C_p = 2C_p$(Mg, hcp_A3)$+C_p$(Ce, fcc_Ce)	Stoichiometric	[4]
Mn–Zn	β_1-MnZn	${}^0\Delta H^{MnZn}_{298.15\ K} = -14{,}000$; ${}^0S^{MnZn}_{298.15\ K} = 63.17$ $C_p = C_p$(α-Mn, cbcc_Mn)$+C_p$(Zn, hcp_Zn)	Stoichiometric	This work
	ζ-$MnZn_{13}$	${}^0\Delta H^{MnZn_{13}}_{298.15\ K} = -22{,}500$; ${}^0S^{MnZn_{13}}_{298.15\ K} = 578.4$ $C_p = C_p$(α-Mn, cbcc_Mn)$+13C_p$(Zn, hcp_Zn)	Stoichiometric	This work
Mg–Zn	Mg_2Zn_{11}	${}^0\Delta H^{Mg_2Zn_{11}}_{298.15\ K} = -85{,}820$; ${}^0S^{Mg_2Zn_{11}}_{298.15\ K} = 499.65$ $Cp = 200 + 0.473\ T - 0.004\ T^2$	Stoichiometric	[11]
	Mg_2Zn_3	${}^0\Delta H^{Mg_2Zn_3}_{298.15K} = -54{,}950$; ${}^0S^{Mg_2Zn_3}_{298.15K} = 183.725$; $Cp = 122 - 0.0311\ T + 0.0001\ T^2$	Stoichiometric	[11]
	$Mg_{12}Zn_{13}$	${}^0\Delta H^{Mg_{12}Zn_{13}}_{298.15\ K} = -250{,}500$; ${}^0S^{Mg_{12}Zn_{13}}_{298.15\ K} = 885.3$ $Cp = 600.5 - 0.10875\ T + 0.0005\ T^2$	Stoichiometric	[11]
	$Mg_{51}Zn_{20}$	${}^0\Delta H^{Mg_{51}Zn_{20}}_{298.15\ K} = 335{,}000.355$; ${}^0S^{Mg_{51}Zn_{20}}_{298.15\ K} = 2510$ $Cp = 51 \times C_p$(Mg, hcp_A3)$+Cp$(Zn, hcp_Zn)	Stoichiometric	[11]

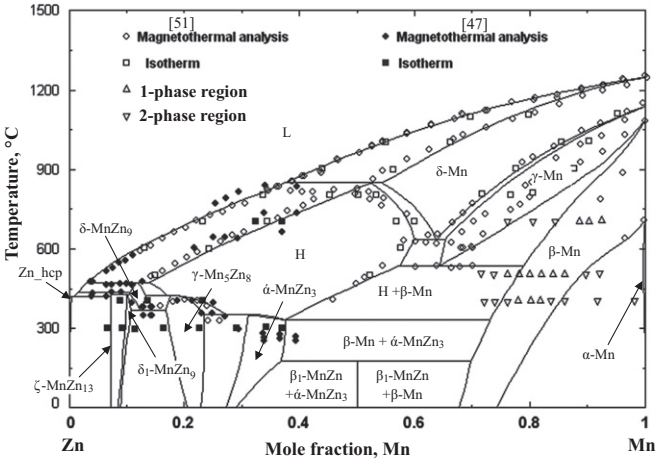

Fig. 2. The calculated Mn–Zn phase diagram along with experimental data points taken from the literature [47,51].

ambiguous portion of the phase diagram, as mentioned by Okamoto and Tanner [54] is the H (denoted as ε in Ref. [54]) phase field. Due to the lack of confirming data this phase is modeled as one wide field in the current work instead of a possible existence of three separate phase fields as suggested by Okamoto and Tanner [54]. For this reason, some of the speculated invariant reactions involving different allotropes of H-phase are not taken into consideration in the current work. The calculated composition of the H/[H+β-Mn] phase transformation at 500 °C is 46.1 at%, reasonably close to the experimentally determined value of 48 at% Zn [49]. The present study estimates the formation temperature of ξ-$MnZn_{13}$ as 433 °C at 92.9 at% Zn, both of which are close to the experimentally determined values of 428 °C, 430 °C [28,47] and 92.9 at% Zn [28]. A very small solubility range of 88–90.8 at% Zn for δ_1-$MnZn_9$ was reported between 350 °C and 424 °C whereas the current study calculates it from 89.3 at% to 90.2 at% Zn. The estimated formation temperature of 425 °C for this phase is very close to the reported value of 424 °C [28]. Good match is also established between the estimated solubility range of 76.6–83.2 at% Zn for γ-Mn_5Zn_8 and that of the experimentally reported value of 77–84.4 at% Zn [26]. According to Schramm's [28] finding, δ-$MnZn_9$ has a composition variation of 86.5–90.6 at% Zn. The current study calculates this as 86.7–89.5 at% Zn and shows reasonable match. The formation temperature of this phase is calculated as 468.5 °C, a little higher than the reported value of 462 °C [28]. The formation temperature of $\acute{\alpha}$-$MnZn_3$ is determined as 348 °C in this study, higher than 325 °C as tentatively proposed temperature [28,54]. The reported Mn-rich solubility limit was 70 at% Zn at both 150 °C and 100 °C, whereas our calculated ones are 65 at% and 67.2 at% Zn, respectively. The transition type phase transformation from $\acute{\alpha}$-$MnZn_3$ to $\acute{\alpha}_1$-$MnZn_3$ reported at −143 °C [54] is not considered in this present study. Though we achieved good consistency for most of the phase boundaries, still there exists a lot of scope for improvement. This may be achieved by new experiments on this system.

The calculated thermodynamic properties are compared with the experimental measurements in Fig. 3(a–c). The activity of Zn in the Mn–Zn liquid measured by Baker et al. [53] is reproduced by the current model as shown in Fig. 3a. The activity of Zn in Mn-rich alloy measured by Dimov et al. [89] at 1300 °C agrees well with the current calculation as shown in Fig. 3b. In Fig. 3c, the calculated activity of Zn in solid Mn–Zn alloys at 420 °C also shows reasonable agreement around 0.2 at% Mn with the measured value of Anantatmula [52].

The Mn–Zn system is a very complex system because of the presence of numerous intermediate compounds with solubility ranges. This made the thermodynamic optimization of this system a challenging task. The latest journal article published on thermodynamic modeling on this system was by Miettinen [1]. For simplification, Miettinen [1] modeled this system only above 400 °C and used Bragg–Williams model to describe the liquid phase. However, the current modeling takes into account all the

Table 7
Invariant points of the Mn–Zn system

Reaction type	Reaction	Composition (at%Zn)			Temp. (°C)	References
Peritectic	L+δ-Mn↔H	62.5	46	48	845	This work
		62	47	50	835	Exp.[28]
		65	50	53	815	Exp. [51]
		65.5	48.1	51.1	815	Calc.[3]
Eutectoid	δ-Mn↔γ-Mn+H	36.3	34.7	40	633	This work
		38	34	42	620	Exp. [51]
		40	35	–	650	Exp. [32]
		37.2	32	42.8	627	Calc.[3]
Eutectoid	γ-Mn↔β-Mn+H	35.7	21.2	42.7	532	This work
		31	25	46	530	Exp. [51]
		35	18		554	Exp. [32]
		33.8	22.4	47.7	530	Calc.[3]
Eutectoid	H↔β-Mn+$MnZn_3$	62.5	27	69	332	This work
		63	–	68.5	~250	Exp.[28]
		62	48	69	220	Exp. [39]
		68.6	29.3	75	282	Calc.[3]
Peritectoid	β-Mn+ά-$MnZn_3$↔β_1-MnZn	0.3	63.1	50	178	This work
		47	70	50	180	Exp. [39]
		31.4	75	50	180	Calc.[3]
Peritectoid	H+γ-Mn_5Zn_8↔ά-$MnZn_3$	70	76	73	350	This work
		72	77	74.50	325	Exp.[28]
		71.7	76	75	325	Calc.[3]
Congruent	H↔γ-Mn_5Zn_8	80.7	80.7		421	This work
		80.8	80.8		400	Exp.[28]
		81.6	81.6		413	Calc.[3]
					420	Exp.[47]
Eutectoid	H↔δ-$MnZn_9$+γ-Mn_5Zn_8	83	87	82.4	418	This work
		85.6	88.9	84.4	350	Exp.[28]
		85	88	84	350	Exp.[47]
		83.9	90	83.11	408	Calc.[3]
Peritectic	L+H↔ δ-$MnZn_9$	97	86.3	88.3	467	This work
		96.3	88.6	90	462	Exp.[28]
		–	88.5	90	462	Exp.[47]
		97.4	87	90	462	Calc.[3]
Peritectic	L+δ-$MnZn_9$ ↔ζ-$MnZn_{13}$	98.7	89.6	93	433	This work
		98.1	90.6	92.7	428	Exp.[28]
		–	90.5	92	430	Exp.[47]
		98.7	90	92.9	428	Calc.[3]
Peritectoid	δ-$MnZn_9$+ζ-$MnZn_{13}$↔δ_1-$MnZn_9$	89.5	93	90	425	This work
		90.6	92.6	90.8	424	Exp.[28]
Eutectic	L ↔ ζ-$MnZn_{13}$+Zn_hcp	99.3	93	99.6	415	This work
		99.3	87.5	100	418	Exp. [21]
		96	80	98	400	Exp. [22]
		99	87.2	100	416	Exp. [23]
		98.9	87.5	99.5	419	Exp. [24]
		99.5	90	100	414	Exp. [25]
		98.6	92.9	99.4	416	Exp.[28]
		99.2	92.7	99.6	417	Calc.[3]
					417	Exp.[29]
					416	Exp.[47]

phases present below and above 400 °C. The liquid phase is described by the MQM and thus makes the system compatible with the other binaries described by the MQM. The only compound, δ-$MnZn_9$, considered by Miettinen [1] was described as line compound. However, a composition variation of 86.5–90.6 at% Zn was found in experimental literature [28]. The present optimization calculates a solubility range of 86.7–89.5 at% Zn for the above phase, reasonably close to the experimental results. Additionally, the eutectic reaction at Zn rich side was mentioned incorrectly (L↔δ-$MnZn_9$+Zn_hcp instead of L↔ζ-$MnZn_{13}$+Zn_hcp) in [1]. Miettinen [1] also described Zn_hcp and H phase by a single Gibbs energy function which resulted in zero solubility for Mn in Zn_hcp. The current work resolves these anomalies observed in Miettinen's [1] work. In addition, the present model considers the solubility ranges reported for γ(Mn_5Zn_8), H, δ($MnZn_9$), δ_1($MnZn_9$) and ά ($MnZn_3$) as suggested by experimental findings [54]. Also, α-Mn is described by Bragg–Williams model in the current work in order to be consistent with the other systems.

4.2. Mg–Mn binary system

Fig. 4 shows the calculated Mg–Mn phase diagram in comparison with experimental phase diagram data of Gröbner et al. [5]

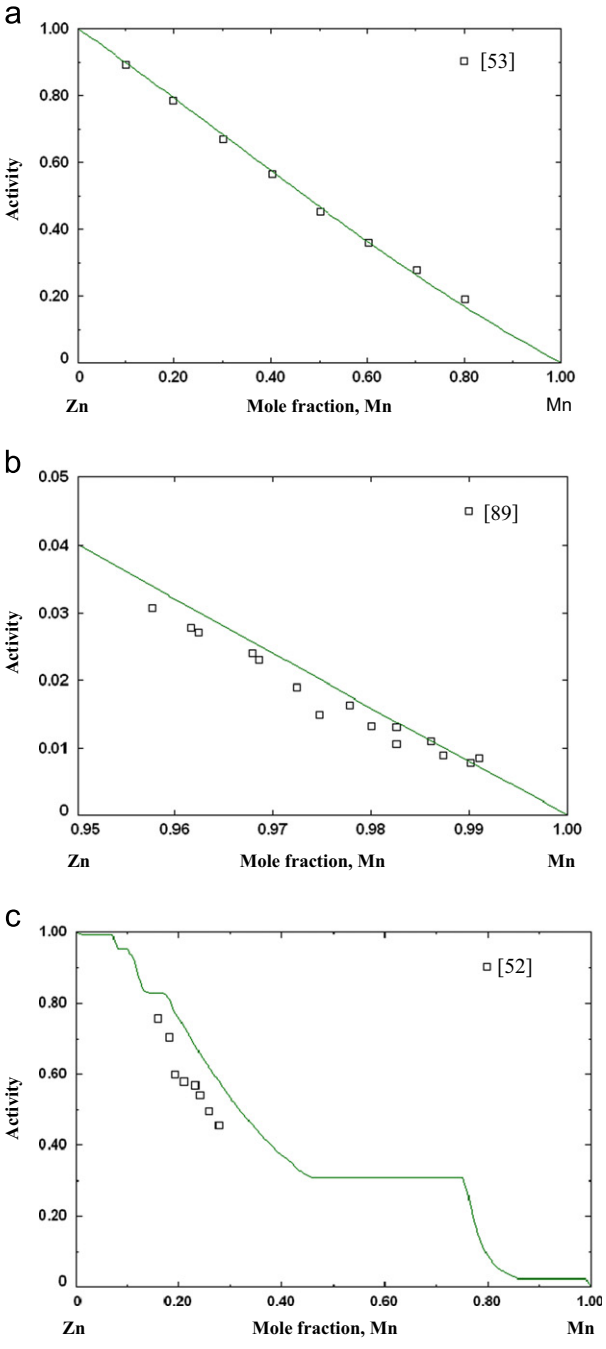

Fig. 3. Calculated activity of Zn (a) in liquid Mn–Zn alloy at 1300 °C, (b) in liquid Mn–Zn alloy at 1250 °C and (c) in solid Mn–Zn alloy at 420 °C along with experimental data. The reference state for Zn is pure liquid Zn.

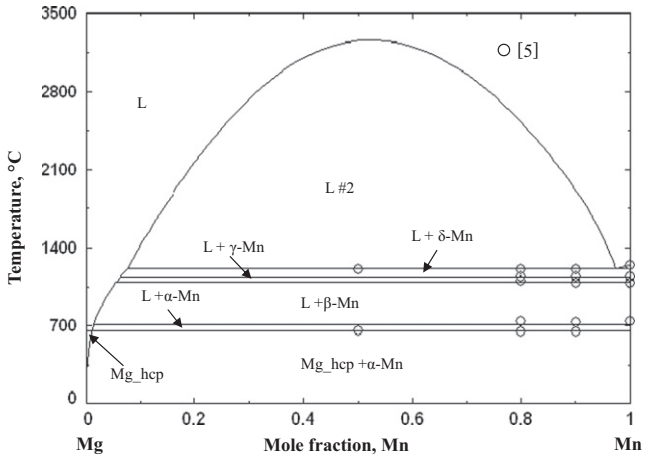

Fig. 4. The calculated Mg–Mn phase diagram along with experimental data from [5].

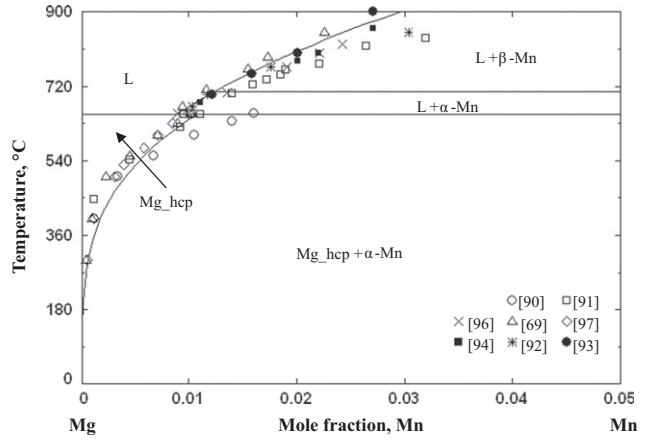

Fig. 5. The calculated Mg-rich part of the Mg–Mn phase diagram along with experimental data from the literature.

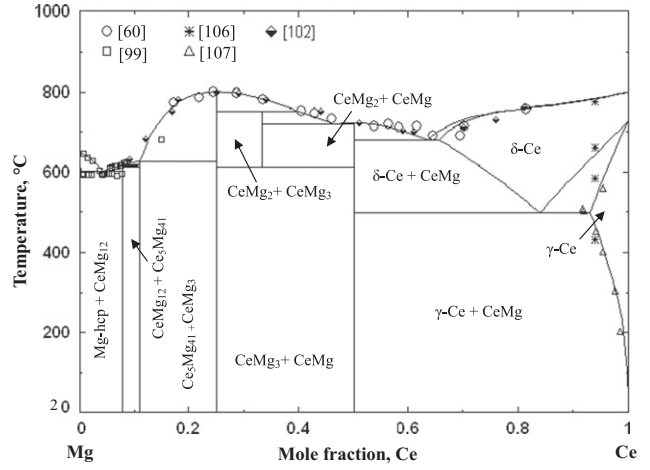

Fig. 6. The calculated Mg–Ce phase diagram in comparison with experimental data from the literature.

who used DTA, SEM and EDS. They [5] reported that the binary monotectic (L↔L+δ-Mn) temperature occurs between 1194 °C and 1202 °C. The current optimization calculates this temperature as 1205 °C, a few degrees higher than the experimental findings. The other transition temperatures measured by Gröbner et al. [5] were 1135–1137 °C for δ-Mn↔L+γ-Mn; 1078–1097 °C for γ-Mn↔L+β-Mn; 706 °C for β-Mn↔L+α-Mn (wrongly written as 731 °C in Table 1 of Ref. [5]) and 642–653 °C for L+α-Mn↔Mg_hcp. The present optimization calculates the above temperatures as 1137 °C, 1084 °C, 706 °C and 650 °C, which are in accord with the findings of Gröbner et al. [5]. Fig. 5 compares the Mg-rich side of the Mg–Mn phase diagram with the data from the literature [90–97]. The calculated solubility of Mn in Mg favors the data of Drits et al. [97], Grogan et al. [91] and Petrov et al. [95] which are self-consistent but deviate from the data of Schmid and Siebel [90] who measured higher Mn solubility in Mg_hcp. Similarly, the liquidus data of Petrov et al. [95] are preferred over Siebel [93] in the present calculation, both of

whom used dip sampling technique but Petrov et al. [95] reported higher liquidus temperature than Siebel [93]. This is based on the suggestion by Hashemi and Clark [55] who pointed out that the dip sampling method has several sources of error that would lower the measured liquidus temperatures and thus the higher liquidus temperatures should be given higher weight during optimization.

The temperature near the equi-atomic position in the miscibility gap in the current study is calculated as 3256 °C. This value is comparable to 3415 °C and 3202 °C, the calculated values of Khan and Medraj [7] and Gröbner et al. [5], respectively. However, higher than 1902 °C, the value calculated by Kang et al. [4]. The Predel's empirical equation estimates this temperature as 2783 °C [7]. The percentage deviation between this value and that calculated by Khan and Medraj [7] and the present calculation are found to be 17.1% and 13.4% (calculation is done by expressing temperature unit in Kelvin). These are well within the percentage deviation of other similar systems [7] estimated in a similar fashion. Khan and Medraj [7] found it more reasonable to evaluate the model on the basis of such thermodynamic considerations rather than to use single experimental information in a specific higher order system to validate the reliability of the calculation in a lower order system as performed by Kang et al. [4]. Except the results of Aniton [57] as obtained in his dissertation, no other relevant experimental information on any other ternary system involving Mg–Mn as a constituent system is available to support the conclusion of Kang et al. [4] that the critical temperature of the Mg–Mn miscibility gap should be far less than that calculated by Predel's equation. Moreover, in a subsequent publication where Antion is one of the co-authors [98], a higher consolute temperature was used. Considering these above facts, the present authors agree with Khan and Medraj [7] and place their calculated consolute temperature close to the value estimated by Predel's equation.

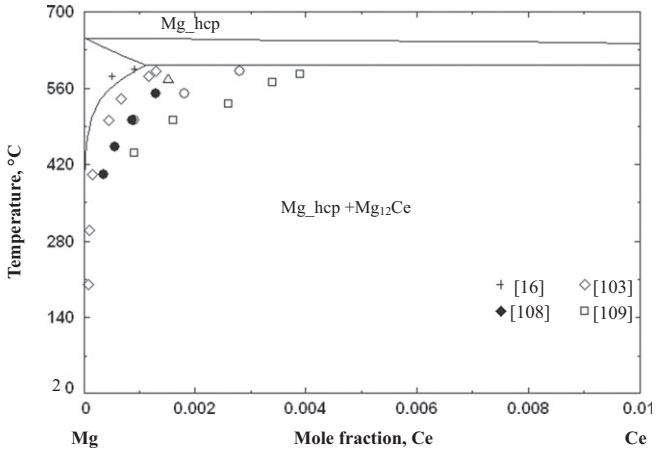

Fig. 7. The calculated Mg–Ce phase diagram near the Mg-rich side vis-à-vis experimental data from literature.

In the present optimization, the consistency of the Mg–Mn system with the available experimental data, especially near the Mg-rich side is improved over [7]; even after using one less model parameter for the liquid as well as the Mg_hcp phase. In addition, α-Mn and β-Mn are described using Bragg–Williams model without compromising their consistency with the experimental data. This has to be done to be consistent with the Mn–Zn system which shows considerable solubility of Zn in these phases, especially in β-Mn. However, in earlier optimizations [4,7] these two were roughly assumed as pure elements.

Table 8
Invariant points of the Mg–Ce system.

Reaction type	Reaction	Composition (at% Ce)			Temp. (°C)	References
Congruent	$L \leftrightarrow Mg_3Ce$	25	25		799	This work
		25	25		796	Exp. [59]
Peritectic	$L + Mg_3Ce \leftrightarrow Mg_2Ce$	39.5	25	33.3	750	This work
		~41	25	33.33	750	Exp. [59]
Congruent	$L \leftrightarrow MgCe$	50	50		721	This work
Peritectic	$L + Mg_3Ce \leftrightarrow Mg_{41}Ce_5$	10.8	25	10.96	625	This work
					635	Exp. [102]
Peritectic	$L + Mg_{41}Ce_5 \leftrightarrow Mg_{17}Ce_2$	8.3	10.96	10.55	617	This work
					621	Exp.[102]
Peritectic	$L + Mg_{17}Ce_2 \leftrightarrow Mg_{12}Ce$	7.3	10.55	7.7	611	This work
					616	Exp.[102]
					597	Calc.[8]
Eutectoid	$Mg_{17}Ce_2 \leftrightarrow Mg_{12}Ce + Mg_{41}Ce_5$	10.55	7.7	10.96	606.6	This work
		8.85	7.7	10.87	611	Exp. [59]
					593	Calc. [8]
Eutectic	$L \leftrightarrow MgCe + \delta\text{-Ce}$	63.4	50	65.6	676	This work
		65	50		688	Exp. [59]
Eutectic	$L \leftrightarrow Mg_{12}Ce + Mg\_hcp$	4.4	10.55	0.11	598	This work
		6.03			585	Exp. [105]
		4.4		0.28	590	Exp.[99]
		3.5		0.09	593	Exp.[16]
		4.3			590	Exp. [101]
		4.2			593	Exp. [102]
		4.3			591 ± 2	Exp. [103]
					594	Exp. [104]
		4.8		0.2	593	Calc. [8]
Eutectoid	$\delta\text{-Ce} \leftrightarrow \gamma\text{-Ce} + MgCe$	84	93	50	498	This work
					490	Exp. [106]
			91.8		505	Exp. [107]

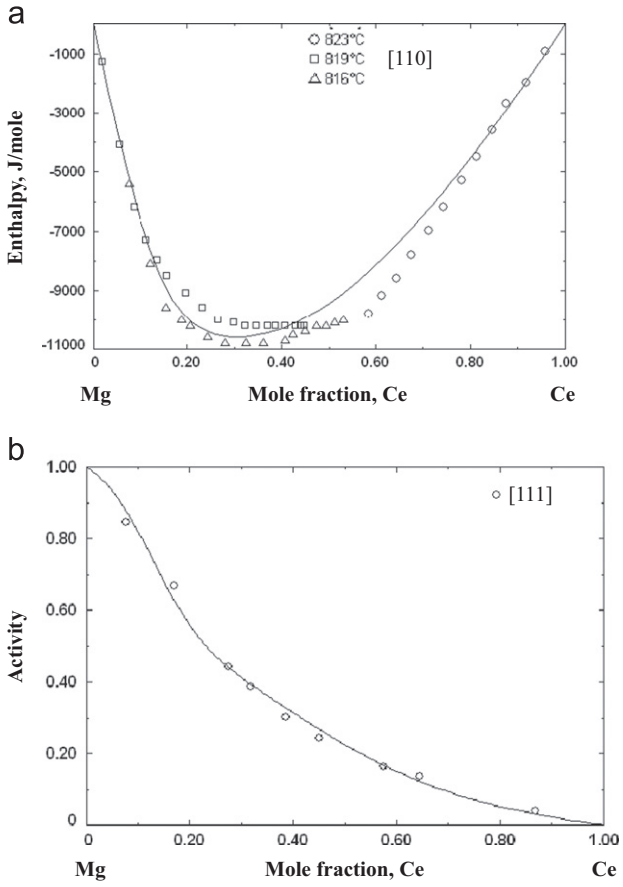

Fig. 8. Calculated (a) enthalpy of mixing at 817 °C and (b) activity of liquid Mg at 860 °C in the liquid Mg–Ce alloys in comparison with experimental data from the literature.

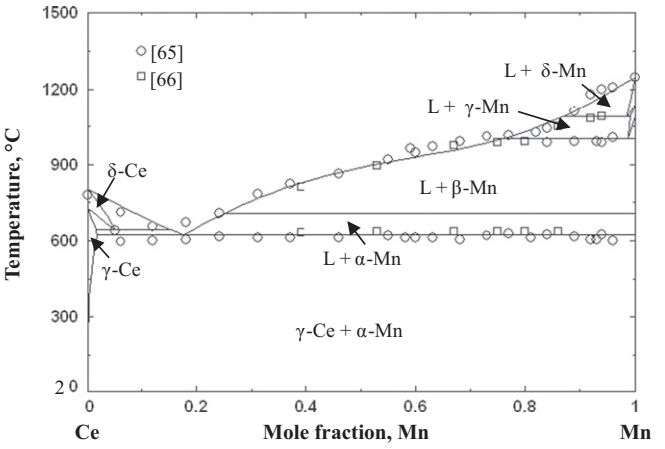

Fig. 9. The calculated Mn–Ce phase diagram in comparison with experimental points from the literature.

4.3. Mg–Ce binary system

In the present optimization of the Mg–Ce system, the model parameters are mostly taken from the work of Kang et al. [4] except for the incorporation of minor but important changes. For instance, the Gibbs energy of the hypothetical phase transformation from pure stable Ce_fcc to unstable Ce_hcp is changed from 5230 J/mol [4] to 8000 J/mol. Both values are able to reproduce the binary with similar consistency. However, the former one results in an artificial stabilization of Mg_hcp phase in the calculated ternary liquidus surface of Mg–Mn–Ce system. The present value is close to the value suggested by Wang et al. [62] derived from first principle calculation at 0 K. Kang et al. [4] reduced this value from 50,000 J/mol [60] to 5230 J/mol to accommodate the observed large solubility of Ce in Y_hcp. However, a value of 8500 J/mol was adopted by Meng et al. [63] and they could successfully reproduce the large solubility of Ce in Y_hcp. Based on these findings, the present optimization adopts a value of 8000 J/mol for this hypothetical transformation. Apart from that, the present optimization modifies model parameters for the γ-Ce and δ-Ce terminal solid solutions used by Kang et al. [4]. However, no extra model parameters are added and even for γ-Ce, only one parameter is used whereas two were used by Kang et al. [4].As stated earlier, Zhang et al. [8] reduced the stability of $Mg_{12}Ce$ by increasing the formation enthalpy from −139,880 J/mol to −137,580 J/mol. This reduces the eutectic temperature of L↔Mg_hcp+$Mg_{12}Ce$ from 601 °C to 593 °C, resulting in the transition temperature to be closer to the reported value between ~590 °C and 594 °C [99–104]. However, this alters the stability of the phases present at the nearby region. For example, $Mg_{17}Ce_2$ becomes stable from 593 °C to 617 °C which is not supported by the experimental findings of [59]. The present calculation yields a eutectic temperature of 598 °C, in between the values reported by Kang et al. [4] and Zhang et al. [8] without compromising the consistency of the other phase regions.

Figs. 6 and 7 show the calculated Mg–Ce phase diagram and the invariant reactions are tabulated in Table 8 along with the experimental data of [16,59,99–109]. A large variation in the experimental solid solubility of Ce in Mg_hcp is observed in the literature [16,99–105]. The present optimization followed the data of Rokhlin [103] who used higher purity Mg and that of Park and Wyman [16] who used longer annealing time to achieve equilibrium. Their findings suggest a relatively low solubility of Ce in Mg_hcp. The rest of the findings of the present calculation show reasonable consistency with the literature data.

The thermodynamic properties of the liquid phase are not discussed further as the model parameters of the liquid phase of Mg–Ce system are directly adopted from Kang et al. [4]. However, for readers' reference, Fig. 8a and b, respectively show the calculated enthalpy of mixing at 817 °C and the activity of Mg at 860 °C in the Mg–Ce liquid in comparison with the experimental data of [110–111].

4.4. Mn–Ce binary system

The calculated Mn–Ce phase diagram is shown in Fig. 9 in relation to experimental data obtained from the literature [65,66]. Calculated vis-à-vis experimental invariant reactions are listed in Table 9. Fig. 10 shows the Ce-rich side of the Mn–Ce phase diagram together with experimental data points measured by other researchers [65,67,68]. The eutectic reaction at the Ce-rich corner (L↔γ-Ce+α-Mn) is calculated at 621 °C which is close to the measured values of 622 ± 2 °C [67] and 621 ± 2 °C [9]. The composition of the liquid for this reaction is calculated at 17.6 at% Mn in the present study, close to the experimental value of 16.1 at% Mn [67]. The other invariant reaction of δ-Ce↔ γ-Ce+L in this Ce-rich region is calculated at 639.4 °C while the experimentally measured values are 638 °C [67] and 640 ± 2 °C [9]. The two invariant reactions near the Mn-rich side, γ-Mn↔ L+β-Mn and δ-Mn↔L+γ-Mn, are calculated as 999 °C and 1087.5 °C, respectively and within ± 2 °C of the experimentally measured values reported in the literature [65,66,112]. The calculated compositions of the invariant reactions are also within ± 2–3 at% from the experimentally measured values as shown clearly in Table 9. Fig. 11 compares the calculated enthalpy of mixing of

Table 9
Invariant points of the Mn–Ce system.

Reaction type	Reaction	Composition (at%Mn)			Temp. (°C)	Reference
Eutectic	L↔γ-Ce+α-Mn	17.6	1.69	100	621	This work
		16.1	~2	~99.5	622 ± 2	Exp.[67]
		16.35	1.53	100	621.6	Calc.[9]
					621 ± 2	Exp.[9]
		17.9	1.9	100	618.7	Calc. [10]
Catatectic	δ-Ce↔γ-Ce+L	5	1.51	15.0	639.4	This work
		5	2	14	638	Exp.[67]
		5	1.36	14.3	638.2	Calc.[9]
					640 ± 2	Exp.[9]
		5.6	1.7	15.4	637.8	Calc. [10]
Catatectic	γ-Mn↔L+β-Mn	98.7	76	100	999	This work
		~96.5	~82.5	~ 99	998	Exp.[112]
		~98	~71	~99.0	998 ± 2	Exp. [65,66]
		96.76	71.74	98.19	997.8	Calc.[9]
					989.4	Calc. [10]
Catatectic	δ-Mn↔L+γ-Mn	98.37	86.9	99.1	1087.5	This work
		~96	87	~98.5	1087	Exp.[112]
		~98	~86	~98.3	1087 ± 2	Exp. [66]
		97.12	84.61	97.79	1087.8	Calc.[9]
					1094	Calc. [10]

the liquid phase at 1327 °C with the reported values [113] and shows good consistency.

As can be seen from the figures and the table, the present optimization reproduced the experimental phase diagram and thermodynamic properties reasonably well. Unlike earlier optimization by Kang et al. [4] employing the MQM for the liquid phase, this study assumed solubility of Mn in both γ-Ce and δ-Ce in accordance with the literature [65,67,68]. The calculated transition temperature (~639 °C) from δ-Ce to γ-Ce is also lower than their calculated value (~724 °C). This is also well supported by the experimental findings of Tang et al. [9] and Thamer [67]. Unlike Ref. [10], the present optimization assumes negligible solubility of Ce in β-Mn due to the lack of any evidence for such solubility in the published literature. Apart from that, δ-Ce and δ-Mn are treated as one Gibbs energy function because of their same crystal structure. An analogous treatment is also applied to the γ-Ce and γ-Mn phases. Table 9 clearly shows that the present optimization yields improved match with the experimental data [65–67,112] over the earlier optimizations [4,9,10].

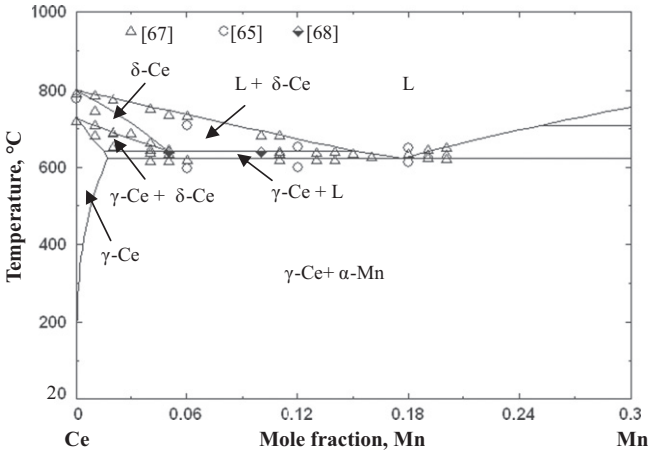

Fig. 10. The calculated Mn–Ce phased diagram near the Ce-rich side with experimental data points from the literature.

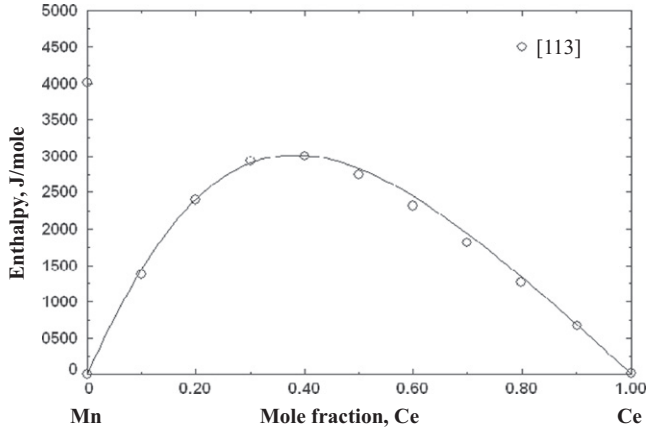

Fig. 11. Calculated enthalpy of mixing of the Mn–Ce liquid at 1327 °C along with experimental data from the literature.

4.5. Mg–Mn–Ce ternary system

As no ternary compounds are known to exist in the Mg–Mn–Ce system, the ternary phase diagram is constructed by extrapolating the constituent binaries. Fig. 12 shows the liquidus surface calculated from the present optimization. A ternary eutectic reaction (L↔Mg_hcp+α-Mn+$CeMg_{12}$) is calculated at 599 °C which agrees with the work of Kang et al. [4]. Figs. 13 and 14 show the calculated vertical sections for constant Ce and Mn, respectively in comparison with experimental data from the literature. The vertical section at 0.3 wt% Ce calculated in the present work matches well with the experimentally measured diagram by Petrov et al. [71] as shown in Fig. 13(a). However, for the 1.6 wt% Ce vertical section, discrepancies are observed between the calculated and experimental diagrams (Fig. 13(b)). Experimental diagram shows the presence of Mg_hcp and (α-Mn+Mg_hcp) phase regions whereas the calculated one does not show these. Instead, the (Mg_hcp+$Mg_{12}Ce$) and (α-Mn+Mg_hcp+$Mg_{12}Ce$) phase regions are seemed to be extended in these regions. It is interesting to note that in the present optimization with increasing Ce percentage from 0.3 wt% to 1.6 wt%, the stability of $Mg_{12}Ce$ compound increases which caused the increase in the (Mg_hcp+$Mg_{12}Ce$) and (α-Mn+Mg_hcp+$Mg_{12}Ce$) phase regions. The same has been observed in the optimization of Kang et al. [4]. Attempts were made to obtain a better consistency between the calculated and experimental Ce-vertical sections. However, this resulted in an

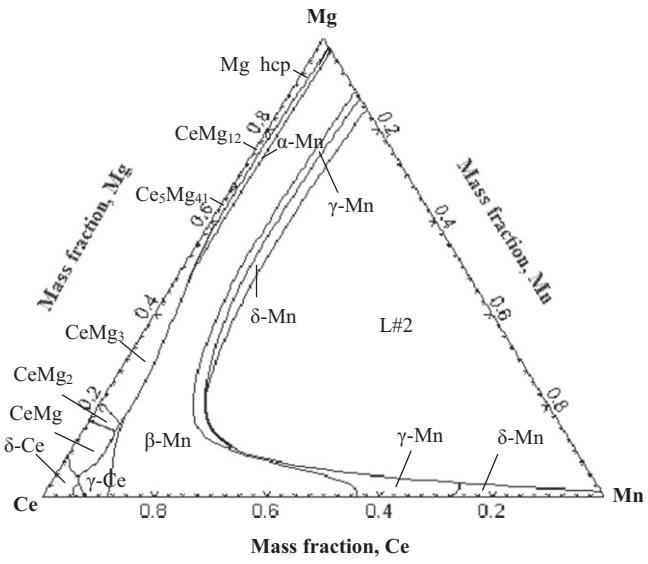

Fig. 12. Calculated liquidus projection of Mg–Mn–Ce ternary.

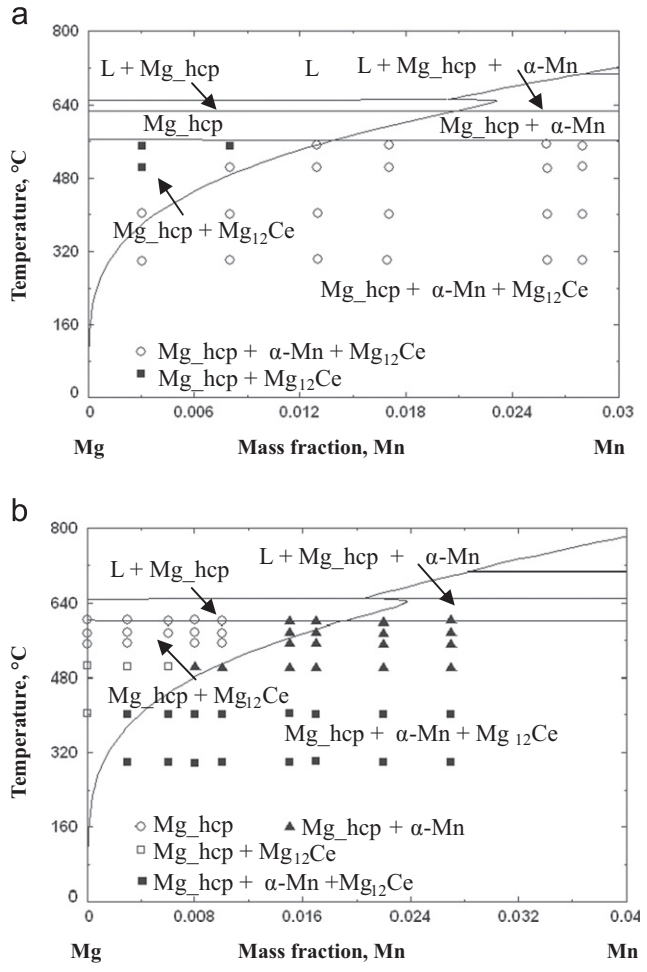

Fig. 13. Calculated vertical sections of (a) 0.3 wt% Ce and (b) 1.6 wt% Ce versus experimental data from the literature [71].

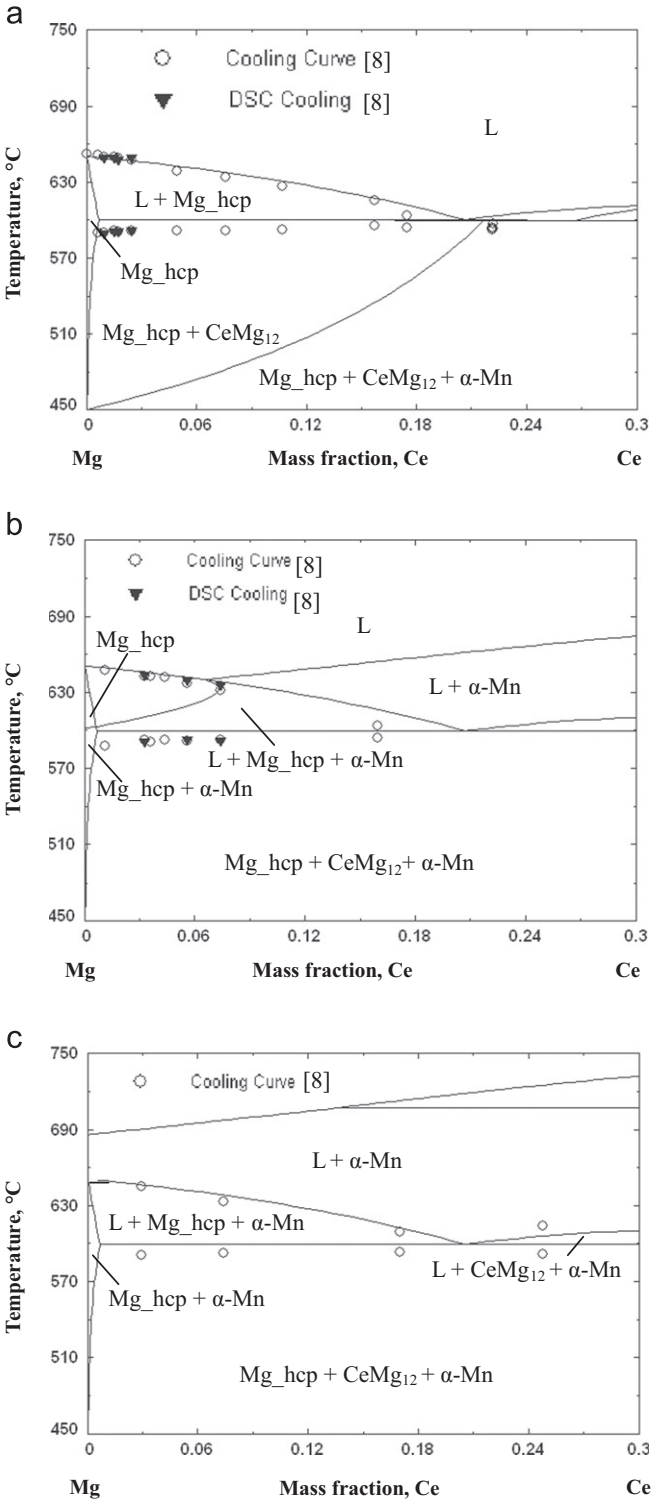

Fig. 14. Calculated vertical sections for (a) 0.6 wt%, (b) 1.8 wt% and (c) 2.5 wt% Mn along with experimental data from the literature.

extended Mg_hcp region in Mg–Ce binary system, contrary to the binary experimental data [15,103]. Unfortunately, no other experimental data are available in the published literature to support or refute the findings of Petrov et al. [71]. However, one will agree with the fact that it is quite difficult to experimentally measure the phases present in very dilute alloys, such as in the present cases which have been more difficult way back in 1957. Though, the present authors do not want to disregard the experimental findings of Petrov et al. [71] based on the mere fact that the experimental results do not match with the calculated ones, but strongly suggest the need of fresh experiments to construct those Ce-vertical sections. Based on the new results, ternary parameters may be added, if needed, to achieve better

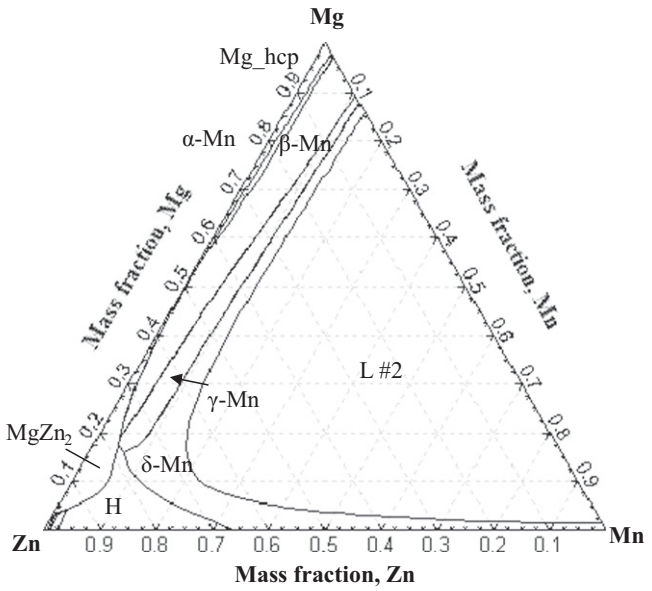

Fig. 15. Calculated liquidus projection of the Mg–Mn–Zn system.

consistency. For the constant Mn vertical sections, the present calculation successfully reproduces the experimental observations reported in [8], except the Liquid + Mg ↔ Mg + $Mg_{12}Ce$—transition temperature calculated at 599 °C which is a little bit higher than the experimental finding which ranges between 590 °C and 595 °C.

4.6. Mg–Mn–Zn ternary system

Very few experimental works on the Mg–Mn–Zn system are available in the literature. Moreover, the data contradict each other. Nevertheless, no ternary compound could be found in the literature. In the present study, the ternary system is thermodynamically described by extrapolating the constituent binaries and subsequently compared with the few available experimental data. No ternary parameter is added to optimize the system. Fig. 15 shows the liquidus surface of the Mg–Mn–Zn system as calculated by the current optimization. Fig. 16 presents the partial liquidus surface of this system near the Mg–Zn edge. The Mg-rich part of this edge is shown in Fig. 16a along with experimental data extracted from the assessed phase diagram by Joel and Schneider [75] and calculated phase boundaries from Ohno and Schmid-Fetzer [78]. The experimental monovariant reaction line for L + Mg_hcp + α-Mn is slightly shifted towards higher Mn side. However, qualitative correlation could be established between the present calculation and the experimental observation [75] as both of them indicated lowering of monovariant reaction line with the addition of Zn. Ohno and Schmid-Fetzer [78] also observed similar trend and a shift between their calculated phase diagram and the diagram assessed by Joel and Schneider [75]. Ohno and Schmid-Fetzer [78] pointed out that Joel and Schneider [75] used a liquid composition with too high Mn content for the L + α-Mn ↔ Mg_hcp reaction in the Mg–Mn system as compared to the recently and more accurate experimental data on the Mg–Mn system [5]. They also argued that the slight almost parallel shift of this line is quite compatible with the experiments [75]. In the present study, the calculated monovariant line is more parallel and closure to the experimental findings of [75] than Ohno and Schmid-Fetzer [78] assessed diagram, indicating higher accuracy of the present thermodynamic description of the system. Fig. 16b shows enlarged portion of the partial liquidus surface near the middle of the Mg–Zn edge. Corresponding invariant reactions are

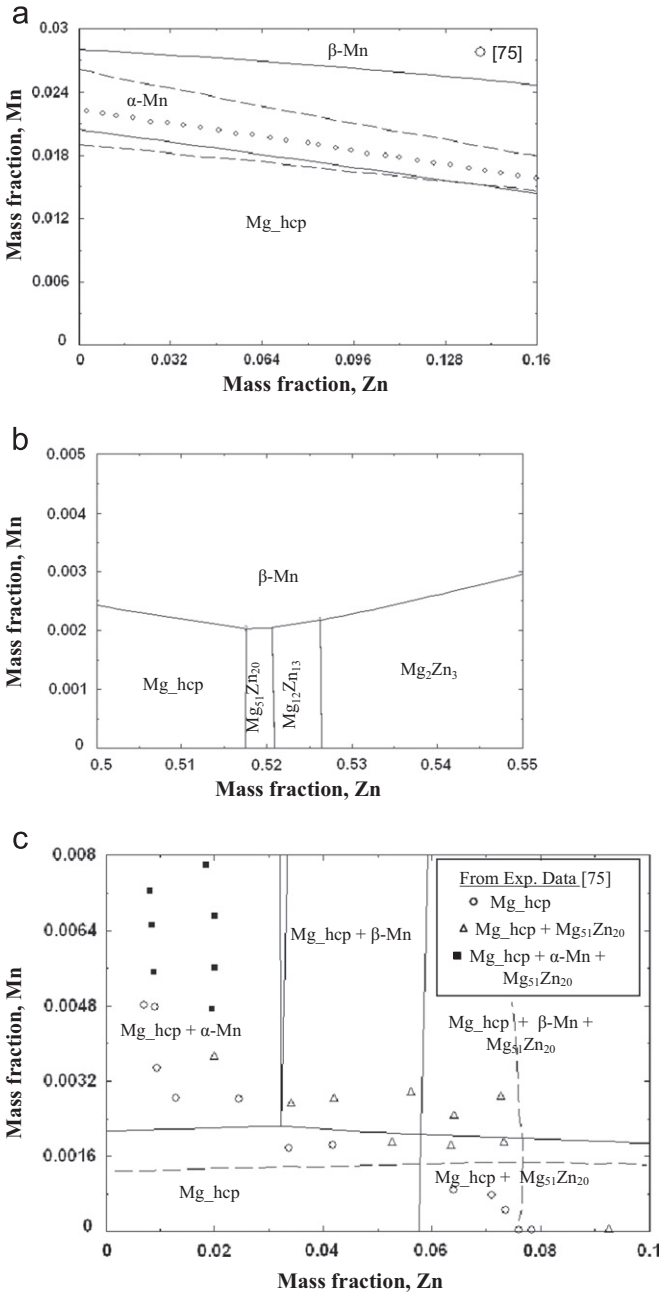

Fig. 16. Near Mg–Zn side of the partial liquidus surface of the Mg–Mn–Zn system; (a) near Mg corner with the experimental monovariant reaction data for L ↔ Mg_hcp + α-Mn from the literature [75] while the dashed lines represent the calculated phase boundaries after [78], (b) near the invariant reaction: L + Mg_hcp ↔ β-Mn + $Mg_{51}Zn_{20}$ and (c) magnified Mg-rich corner just below the invariant reaction temperature of 342.8 °C of L + Mg_hcp ↔ β-Mn + $Mg_{51}Zn_{20}$ in comparison with the experimental data from [75]. The dashed line signifies the phase boundaries calculated by [78]. The above invariant reaction was estimated at 347 °C and 340.18 °C by Refs. [75,78], respectively.

listed in Table 10. The transition temperature of L + Mg_hcp ↔ β-Mn + $Mg_{51}Zn_{20}$ has been calculated as 343 °C; in between the calculated 341 °C [78] and experimental 347 °C [75] findings. However, the Mn is detected as β-Mn (i.e., Mn_cub) in the present calculation instead of α-Mn (Mn_cbcc) as calculated by Ohno and Schmid-Fetzer [78]. This is because in the present calculation the α-Mn region extends up to 40 wt% Zn while it ended at 55 wt% Zn in the calculation of [78]. Fig. 16c shows the magnified Mg-rich corner just below this invariant reaction at 342 °C. Experimental data in this region [75] and assessed phase boundaries from [78]

Table 10
Invariant reactions in the Mg–Mn–Zn system, near the middle of the Mg–Zn edge

Reaction type	Reaction	Composition of liquid, wt%			Temp (°C)	References
		Mn	Mg	Zn		
Ternary quasi-peritectic	$L+Mg\_hcp \leftrightarrow \beta\text{-}Mn+Mg_{51}Zn_{20}$	0.2	48.0	51.8	342.82	This work
		0.2	47.5	52.3	340.18	Calc.[78]
					347	Exp.[76]
Ternary eutectic	$L \leftrightarrow \beta\text{-}Mn+Mg_{51}Zn_{20}+Mg_{12}Zn_{13}$	0.20	47.74	52.06	342.79	This work
		0.25	47.41	52.34	340.16	Calc.[78]
Ternary quasi-peritectic	$L+Mg_2Zn_3 \leftrightarrow Mg_{51}Zn_{20}+Mg_{12}Zn_{13}$	0.22	47.18	52.6	346.40	This work

also plotted on the same diagram. The experimental data of [75] correspond to 347 °C whereas assessed value of [78] is at 340 °C. Present calculation shows the Mg_hcp phase field extended towards higher Mn concentration but lower at Zn side as compared to [78]. None of the assessed diagrams (the present work as well as that of Ref. [78]) shows good match with the experimental findings. However, the experimental data reported by [75] is inconsistent and seemed to be unreliable. For example, they [75] claimed to have a wider presence of $Mg_{51}Zn_{20}$, even for a very low concentration of Zn. However, the present assessment shows presence of Mg_hcp+α-Mn in that region and supported by the calculation of [78]. Ohno and Schmid-Fetzer [78] pointed out that this could be due to absence of a proper equilibrium condition during experimentation [75]. Nonetheless, more experimental work is required to have a better understanding of the phase relationships in this region. The Zn-rich corner of the liquidus surface is magnified and presented in Fig. 17. Experimental information does not exist for this region too. Several isothermal sections are calculated and shown in Fig. 18 in comparison with available experimental data [76]. It can be seen from these figures that the present calculation always yields lower solubility than what is reported in the experimental results of Bumazhnov [76] who measured the solubilities by microstructural analysis. Detecting trace compositions in small sized particles by microstructural observation is often associated with high difficulties and this could have caused determination of higher solubility than the actual values [78]. Further, when the weight fraction of Zn approaches zero, the experimental observation by Bumazhnov [76] does not approach to the solubility limit of the Mg–Mn binary system as pointed out in Ohno and Schmid-Fetzer [78]. Bumazhnov [76] and Joel and Schneider [75] both reported that the Mn solubility in Mg_hcp decreases with increasing Zn composition, although their data provide quantitatively different results. Ohno and Schmid-Fetzer [78] questioned this consistency suspecting it to be the result of possible non-equilibrium effect in these two experimental works. The current calculation estimates almost constant solubility of Mn in Mg_hcp with increasing Zn, similar to the calculated results of [78]. Fig. 19 shows the calculated vertical section near the Mg-rich side for 0.02 wt% Mn. In this figure, the bold solid line is the boundary between Mg_hcp/[Mg_hcp+Liquid] from the present calculation and the dashed line represents the same from Ohno and Schmid-Fetzer's calculation [78]. The solid triangles are the experimentally determined incipient melting temperatures (or solidification temperatures) for Mg–Mn–Zn cast alloy with 0.02 wt% Mn by Busk and Marande [79]. As one can see from the figure that the present calculation yields a result where calculated solidification temperatures for lower Zn content are lower than the experimental ones and just the opposite for higher Zn content (more than 3 wt% Zn). However, the gap becomes less with increasing Zn content. On the contrary, the assessed diagram by Ohno and Schmid-Fetzer's calculation [78] showed very good match for low Zn content but poor match for higher Zn content. They argued that this is because that at lower Zn content the solidification process is closure to the equilibrium condition but as Zn concentration

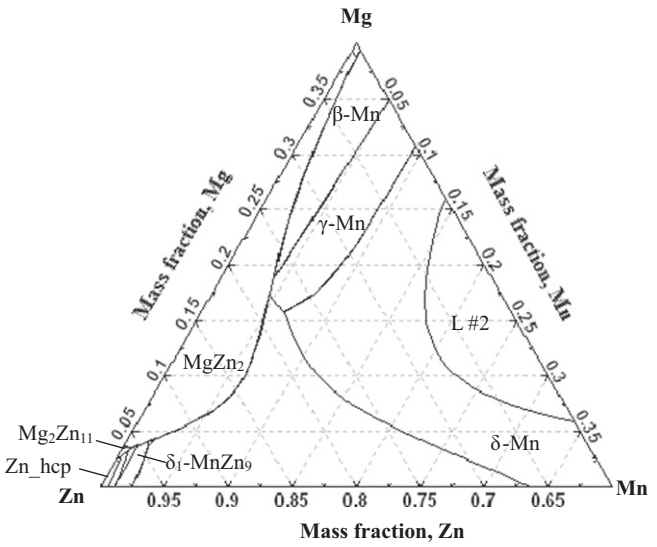

Fig. 17. Calculated Zn-rich corner of the liquidus projection of the Mg–Mn–Zn system.

increases, it becomes more like Scheil conditions. They also calculated solidification temperatures according to Scheil condition and showed that at higher Zn concentration, experimentally determined and Scheil's calculated temperatures match very well with each other. Busk and Marande [79] determined these solidification temperatures based on tensile testing during stepwise heating where a critical amount of liquid must be present to the observed brittle fracture. It is thus expected that the experimental data always take a slightly higher value than the calculated equilibrium temperatures. Also, at low Zn composition range, the detection of small amount of residual liquid results in a large uncertainty in the measured solidification temperatures. Thus the present calculation which shows lower solidification temperatures and higher gap from the experimentally measured temperatures is quite justified. With increasing Zn concentration, more and more solid state diffusion is required to attain equilibrium which could not be attained in sand-mold casting. This resulted in determination of lower solidification temperatures by Busk and Marande [79] in higher Zn concentration range. This agreement is also supported by the fact that at this Zn concentration range, Scheil's calculation matches well with the experimental values, suggesting the solidification process took place at non-equilibrium conditions. In this range, the present calculation yields values between the experimentally determined ones [79] and that of assessed by Ohno and Schmid-Fetzer's [78].

5. Summary

In the present optimization five binaries are investigated (i.e., Mg–Ce, Mg–Mn, Mg–Zn, Mn–Zn and Mn–Ce) and subsequently

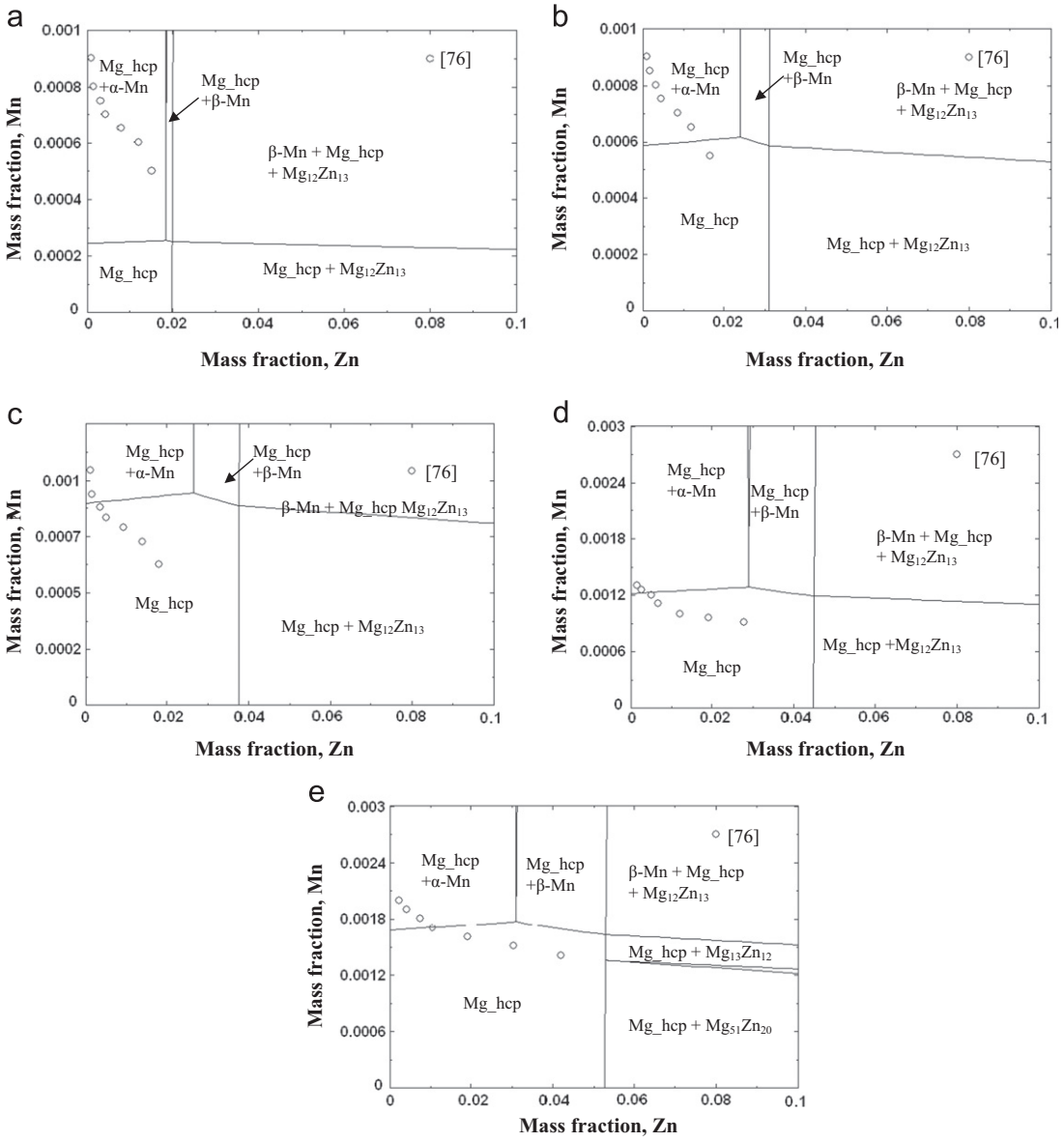

Fig. 18. The Mg-rich corner of the calculated isothermal sections at (a) 200 °C, (b) 250 °C, (c) 275 °C, (d) 300 °C and (e) 325 °C along with experimental points for Mg solubility from the literature.

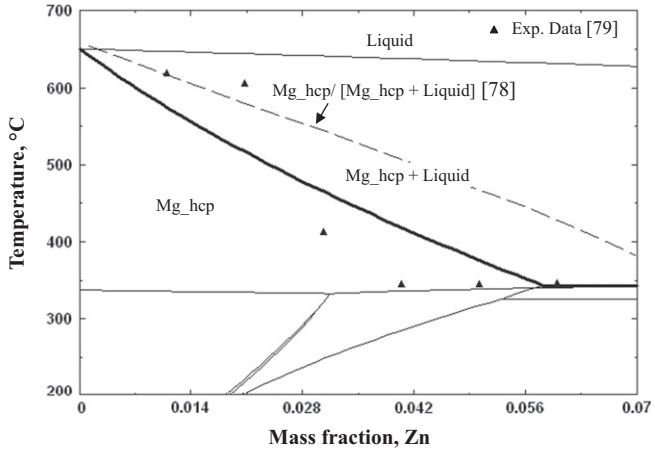

Fig. 19. Zn composition dependence of the incipient melting temperature of as-cast Mg–Mn–Zn alloys containing 0.2 wt% Mn presented by solid triangles in Ref. [79]. The bold black line represent the boundary between Mg_hcp/[Mg_hcp + Liquid] from present calculation and the dashed line represents the same from Ref. [78].

extrapolated to construct two ternaries, Mg–Mn–Ce and Mg–Mn–Zn, without adding any ternary parameters. The whole idea of this present work is to improve the thermodynamic description of the existing systems by incorporating as much as experimental data from the literature as possible. However, care is taken to keep the number of model parameters at the lowest and if and when possible to stick with the model parameters of the earlier works. The latter part is given importance as the earlier description of the binary of interest has already been successful to describe a ternary system with some different elements. A huge change in model parameters of a binary system (especially in case of liquid phase) to describe a new ternary system might make the already modeled ternaries that used these binary parameters (as published in earlier works) quite off. This has become more important as in most of the cases; experimental data on the ternaries are sparse. Nevertheless, the followings are the salient features of the present work:

1. Mn–Zn system not only is modeled using the MQM but also improved a lot over the previous assessment. For the first time,

the Mn–Zn system is optimized taking into account the solubility ranges of almost all the compounds. Good agreement is found between the calculated and the experimental observations considering the complexity of the system.

2. The concerns/issues found in previous assessment of the concerned binaries are addressed and changes are made accordingly. For example, the value of Gibbs energy of the hypothetical phase transformation of pure Ce from stable FCC to unstable HCP is modified along with the changes for the model parameters of the γ-Ce and δ-Ce terminal solid solutions. In the case of the Mn-Ce system, the solubility of Mn in γ-Ce and δ-Ce was not considered in the earlier optimization [4]. In the present study this is accounted for and the system is re-optimized. The consistency of the Mg–Mn system is improved over the last recent publication [7] and controversial issue on the consolute temperature of the liquid miscibility gap is addressed.
3. Most of the time, the improved thermodynamic description of the binaries has been achieved using less number of parameters than the previous assessments.
4. All the terminal solid solutions in the binary systems are modeled using Bragg–Williams random solution model. Terminal solid solutions with the same crystal structures are described using one single Gibbs' energy function. Although this has made the present optimization process more complicated and difficult to reproduce the experimental results, it had to be done because it is more physically sound. This has been achieved without compromising the consistency with the experimental data.
5. In order to verify the quality of the thermodynamic re-optimization, the modified binaries are extrapolated to construct the Mg–Mn–(Ce, Zn) ternaries and compared with the available experimental data.
6. The present optimization achieves better consistency with the experimental data for the Mg–Mn–Zn and Mg–Mn–Ce systems than the previous assessments.
7. Being two important members in the Mg-alloys system, the Mg–Mn–Ce and Mg–Mn–Zn should be studied experimentally in more detail. Based on the new experimental data, the present optimization can be further refined.

Appendix A. Supporting information

Supplementary data associated with this article can be found in the online version at http://dx.doi.org/10.1016/j.calphad.2013.01.008.

References

[1] J. Miettinen, Thermodynamic description of the Cu–Mn–Zn system in the copper rich corner, CALPHAD 28 (2004) 313–320.
[2] A.D. Pelton, S.A. Degterov, G. Eriksson, C. Robelin, Y. Dessureault, The modified quasichemical model I-Binary solutions, Metall. Mater. Trans. B 31B (2000) 651–659.
[3] M.A. Khan Thermodynamic Modeling of the Mg–Mn–(Al, Zn) Systems, MASc Thesis, Concordia University, 2009.
[4] Y.-B. Kang, A.D. Pelton, P. Chartrand, P. Spencer, C.D. Fuerst, J. Phase Equilib. Diffus. 28 (2007) 342–354.
[5] J. Gröbner, D. Mirkovic, M. Ohno, R. Schmid-Fetzer, Experimental investigation and thermodynamic calculation of binary Mg–Mn phase equilibria, J. Phase. Equilib. Diffus. 26 (2005) 234–239.
[6] J. Tibbals Mg–Mn system. In: COST 507–Thermochemical Database for Light Metal Alloys, I. Ansara, A. T. Dinsdale, and M. H. Rand, Eds., (1998), 2, EUR 18499, pp. 215–217.
[7] M.A. Khan, M. Medraj, Thermodynamic description of the Mg–Mn, Al–Mn and Mg–Al systems using the modified quasi-chemical model for the liquid phases, Mater. Trans., JIM 50 (2009) 1113–1122.
[8] X. Zhang, D. Kevorkov, I.H. Jung, M. Pekguleryuz, Phase equilibria on the ternary Mg–Mn–Ce system at the Mg-rich corner, J. Alloys Compd. 482 (2009) 420–428.
[9] C. Tang, Y. Du, L. Zhang, H. Xu, Z. Zhu, Thermodynamic assessment of the Ce–Mn system, J. Alloys Compd. 437 (2007) 102–106.
[10] J. Kim, I.H. Jung, Critical systematic evaluation and thermodynamic optimization of the Mn–RE system: RE=La, Ce, Pr, Nd and Sm, J. Alloys Compd. 525 (2012) 191–201.
[11] P. Ghosh, M.M. Islam, M. Medraj, Critical assessment and thermodynamic modeling of Mg–Zn, Mg–Sn, Sn–Zn and Mg–Sn–Zn system, CALPHAD 36 (2012) 28–43.
[12] R.J. Chadwick, The constitution of the alloys of magnesium and zinc, J. Inst. Met. 449 (1928) 285–299.
[13] W. Hume-Rothery, E.D. Rounsefell, The system magnesium–zinc, J. Inst. Met. 41 (1929) 119–138.
[14] G. Grube, Alloys of magnesium with cadmium, zinc, bismuth and antimony, Z. Anorg. Chem. 49 (1906) 72–92.
[15] G. Bruni, C. Sandonnini, E. Quercigh, The ternary of magnesium, zinc and cadmium, Z. Anorg. Chem. 68 (1911) 73–90.
[16] J.J. Park, L.L. Wyman Phase Relationship in Mg Alloys, WADC Technical Report 1957, 57–504: Astia Document no. AD142110, pp.1–33.
[17] G. Grube, A. Burkhardt, The electrical conductivity, thermal expansion and hardness of magnesium–zinc, Z. Elektrochem. Angew. Phys. Chem. 35 (1929) 315–331.
[18] H. Adenstedt, J.R. Burns, The determination of solidus temperature in magnesium alloys by dilatometric measurements, Trans. A.S.M. 43 (1951) 873–887.
[19] W. Schmidt, M. Hansen, Solidus and solvus of the magnesium solid solution of magnesium–zinc alloys, Z. Metallkd. 19 (1927) 452–455.
[20] D.J. Chakraborty, D.E. Laughlin, The Cu–Ir System, Bull. Alloy Phase. Diagr. 8 (1987) 132–136.
[21] N. Parravano, U. Perret, The alloys of zinc and manganese, Gazz. Chim. Ital. 45 (I) (1914) 1–6.
[22] P. Gieren, Cast alloys of zinc with special consideration on their utilization as bushing metals, Z. Metallkd. 11 (1919) 14–22.
[23] P. Siebe, Manganese–bismuth, manganese–zinc and manganese–silver alloys, Z. Anorg. Allg. Chem. 108 (1919) 161–183.
[24] W. Peirce, Studies on the constitution of binary zinc-base alloys., Trans. Metall. Soc. AIME 63 (1923) 767–795.
[25] C. Ackermann, The binary system manganese–zinc, Z. Metallkd. 19 (1927) 200–204.
[26] N. Parravano, V. Caglioti, Structure and chemical composition of some [manganese–zinc and cobalt–zinc] alloys, Mem. Accad. Italia Chim. 3 (3) (1932) 5–21.
[27] N. Parravano, V. Caglioti, Further investigations of the alloys of zinc and manganese, Ric. Sci. 7 (I I) (1936) 223–224.
[28] J. Schramm, The system manganese–zinc with 0–50% Mn, Z. Metallkd. 32 (1940) 399–407.
[29] E. Weisse, A. Blumenthal, H. Hanemann, Results of a study of eutectic Zn alloys, Z. Metallkd. 34 (1942) 221.
[30] K. Moeller, X-ray and microscopic studies with quaternary Zn–Mn–Cu–Ag alloys, Z. Metallkd. 35 (1943) 27–28.
[31] G. Edmunds, Liquidus determinations in Zn-rich alloys (Zn–Fe; Zn–Cu; Zn–Mn), Trans. Metall. Soc. AIME 156 (1944) 263–276.
[32] E. Potter, R. Huber, Manganese–zinc phase diagram from 0 to 50% zinc., Trans. Am. Soc. Metall. 41 (1949) 1001–1022.
[33] U. Zwicker, γ-Phase of manganese, Z. Metallkd. 42 (1951) 246–252.
[34] H. Nowotny, R. Bittner, Contribution to the problem of anomalous diamagnetism, Monatsh. Chem 81 (1950) 898–901.
[35] S. Tezuka, S. Sakai, Y. Nakagawa, Ferromagnetism of Mn–Zn alloy, J. Phys. Soc. Jpn. 15 (1960) 931.
[36] P. Brown, The structure of the ζ-phase in the transition metal-zinc alloy systems, Acta. Crystallogr. 15 (1962) 608–612.
[37] Y. Nakagawa, T. Hori, Magnetic transition and crystal distortion in MnHg and $MnZn_3$, J. Phys. Soc. Jpn. 17 (1962) 1313–1314.
[38] Y. Nakagawa, T. Hori, Neutron diffraction studies of Mn–Zn alloys, J. Phys. Soc. Jpn. 19 (1964) 2082–2087.
[39] Y. Nakagawa, T. Hori, Phase diagram of manganese–zinc system, Trans. Jpn. Inst. Metall. 13 (1972) 167–170.
[40] Y. Nakagawa, S. Sakai, T. Hori, Magnetic properties of Mn–Zn alloys, J. Phys. Soc. Jpn. 17 (1962) 168–171, Suppl. B-I.
[41] B. Henderson, R. Willcox, Lattice spacing relations in hexagonal close-packed silver–zinc–manganese alloys, Philos. Mag. 9 (1964) 829–846.
[42] T. Hori, Y. Nakagawa, A new ferromagnetic phase in Mn–Zn alloy system, J. Phys. Soc. Jpn. 19 (1964) 1255.
[43] T. Hori, Y. Nakagawa, J. Sakurai, Magnetization and magnetic structure of manganese–zinc and manganese–zinc–gallium alloys of cesium chlorine-type structure, J. Phys. Soc. Jpn. 24 (1968) 971–976.
[44] D. Martin, The specific heat of zinc–manganese alloys, Ann. Acad. Sci. Fenn. Ser. A. 210 (1966) 140.
[45] D. Martin, Specific heat of pure zinc and some zinc–manganese alloys, Phys. Rev. 167 (1968) 640–651.
[46] D. Martin, Specific heat of pure zinc and dilute zinc–manganese alloys below 5°K, Phys. Rev 186 (1969) 642–648.
[47] E. Wachtel, K. Tsiuplakis, Magnetic properties of zinc-rich zinc–manganese alloys in the liquid and solid state, Z. Metallkd. 58 (1967) 41–45.

[48] H. Uchishiba, T. Hori, Y. Nakagawa, Cubic–tetragonal transition and antiferromagnetism of ά-$MnZn_3$, J. Phys. Soc. Jap. 27 (1969) 600–604.
[49] A. Farrar, H. King, Axial ratios and solubility limits of hcp η and ε phases in the systems cadmium–manganese and zinc–manganese, Metallography 3 (1970) 61–70.
[50] B. Lyazgin, G. Kazantsev, V. Lebedev, I. Nichkov, S. Raspopin, L. Martem'yanov, Thermodynamic properties of the manganese–zinc system, Zh. Fiz. Khim. 45 (1971) 1976–1978.
[51] O. Romer, E. Wachtel, Constitution of the zinc–manganese and the zinc–manganese–aluminum systems, Z. Metallkd. 62 (1971) 820–825.
[52] R. Anantatmula, Brillouin zone effects in ζ phase alloys of the manganese–zinc system, Scr. Metall. 9 (1975) 223–228.
[53] E. Baker, Thermodynamic activities in the zinc–manganese system at 1250 °C, Z. Metallkd. 71 (1980) 760–762.
[54] H. Okamoto, L. Tanner, The Mn–Zn (manganese–zinc) system, Bull. alloy. phase diagr. 11 (1990) 377–384.
[55] A. Hashemi, J. Clark, The Mg–Mn (magnesium–manganese) system, Bull. alloy. phase. diagr. 6 (1985) 160–164.
[56] H. Okamoto, Magnesium–manganese binary alloy phase diagram, J. Phase Equilib. Diffus. 29 (2008) 208.
[57] C. Antion, Etude du system Mg–Mn–Y–Gd et Development D'alliages de Magnesium Pour des Applications Structurales a Chaud, these Docteur de L'INPG, Institut National Polytechnique de Grenoble (2003).
[58] B. Predel, Constitution and thermodynamics of systems with miscibility gaps, Z. Metallkd. 56 (1965) 791–798.
[59] A.A. Nayeb-Hashemi, J.B. Clark, The Ce–Mg (cerium–magnesium) system, Bull. Alloy Phase diagr. 9 (1988) 162–172.
[60] G. Cacciamani, A. Saccone, R. Ferro Ce–Mg system, In: COST 507—Thermochemical Databases for Light Metal Alloys, I. Ansara, A. T. Dinsdale, and M.H. Rand, Eds., Vol. 2, EUR 18499, 1988, pp. 137–140.
[61] X. Zhang, D. Kevorkov, M. Pekguleryuz, Stoichiometry study on the binary compounds in the Mg–Ce system-Part I, J. Alloys Compd. 475 (2009) 361–367.
[62] Y. Wang, S. Curtarolo, C. Jiang, R. Arroyave, T. Wang, G. Ceder, L.Q. Chen, Z.Q. Liu, Ab initio lattice stability in comparison with CALPHAD lattice stability, CALPHAD 28 (2004) 79–90.
[63] F.H. Meng, L.B. Liu, H.S. Liu, Z.P. Jin, Thermodynamic assessment of the Ce–Y system, CALPHAD 30 (2006) 323–325.
[64] L. Rolla, A. Iandelli, Contribution to the knowledge of rare earth metals and their compounds: the La–Mn alloys, Ber. Deut. Chem. Ges. 75 (1942) 2091–2095.
[65] A. Iandelli, The Ce–Mn alloys, Atti. Accad. Naz. Lincei. Rend. 13 (1952) 265–268. (Equi. Diagram; Experimental).
[66] M.S. Mirgalovskaya, I.A. Strel'nikova, Investigation in the Mn–Ce system, Trudy Inst. Met. im A.A. Baikova Akad. nuk. SSSR. 2 (1957) 135–138.
[67] B.J. Thamer, The system cerium–manganese in the range of 0–20 atomic per cent manganese, J. Less-Common Met. 7 (1964) 341–346.
[68] R.H. Perkins, L.A. Geoffrion, J.C. Biery, Densities of some low melting cerium alloys, Metall. Trans. AIME 233 (1965) 1703–1710.
[69] C. Tang, Y. Du, H. Xu, S. Hao, L. Zhang, Study on the non-existence of liquid miscibility gap in the Ce–Mn system, J. Min. Metall. 43B (2007) 21–28.
[70] V.I. Mikheeva, Izv Sectora Fiz.-Khim Anal 19 (1949) 429–436.
[71] D.A. Petrov, M.S. Mirgalovskaya, I.A. Strelnikova, E.M. Komova, The constitution diagram for the magnesium–manganese system, Trudy Baikov Inst. Metall. 1 (1957) 144–147.
[72] M.V. Chukhrov, Z.N. Khrisanova, Metall. Term. Obrab. Metallov. 12 (1980) 46–48.
[73] Y.B. Kang, A.D. Pelton, P. Chartrand, P. Sepncer, C.D. Fuerst, Thermodynamic database development of the Mg–Ce–Mn–Y system for Mg alloy design, Metall. Mater. Trans. A 38A (2007) 1231–1243.
[74] X. Zhang, D. Kevorkov, M. Pekguleryuz, Study on the intermetallic phases in the Mg–Ce system: Part II. Diffusion couple investigation, J. Alloys Compd. 501 (2010) 366–370.
[75] H. Joel, A. Schneider, Magnesium–manganese–zinc (–silicon–titanium) alloy, Metallurgy 22 (3) (1968) 193–199.
[76] F. Bumazhnov, Physiochochemical investigation at varied temperatures of solubility of zinc and manganese in magnesium., Izvestiya Vysshikh Uchebnykh Zavedenii Tsvetn. Met. (Moscow) 2 (1960) 138–143.
[77] G. Raynor, Constitution of ternary and some complex alloys of magnesium, Int. Met. Rev. 216 (1977) 65–96.
[78] M. Ohno, R. Schmid-Fetzer, Mg-rich phase equilibria of Mg–Mn–Zn alloys analyzed by computational thermochemistry, Int. J. Mater. Res. 97 (2006) 526–532.
[79] R.S. Busk, R.F. Marande, Trans. Am. Inst. Min. Metall. Pet. Eng. 166 (1946) 346–368.
[80] A.T. Dinsdale, Thermodynamic data for the elements, CALPHAD 15 (1991) 317–425.
[81] P.J. Spencer, A.D. Pelton, Y.-B. Kang, P. Chartrand, C.D. Fuerst, Thermodynamic assessment of the Ca–Zn, Sr–Zn, Y–Zn and Ce–Zn system, CALPHAD 32 (2008) 423–431.
[82] F. Sommer, Association model for the description of thermodynamic functions of liquid alloys II. Numerical treatment and results, Z. Metallkd. 73 (1982) 77–86.
[83] A.D. Pelton, Y-B. Kang, Modeling short-range ordering in solutions, Int. J. Mater. Res. 98 (2007) 1–10.
[84] A.D. Pelton, P. Chartrand, The modified quasi-chemical model, Metall. Mater. Trans. A 32A (2001) 1355–1360.
[85] O. Redlich, A.T. Kister, Thermodynamics of nonelectrolyte solutions, X–Y–T relations in a binary system, J. Ind. Eng. Chem. Washington D. C. 40 (1948) 341–345.
[86] J.O. Andersson, A. Guillermet, M. Hillert, B. Jansson, B. Sundman, A compound-energy model of ordering in a phase with sites of different coordination numbers, Acta Metall. 34 (1986) 43–45.
[87] M. Hillert, The compound energy formalism, J. Alloys Compd. 320 (2001) 161–176.
[88] F. Kohler, Estimation of the thermodynamic data for a ternary system from the corresponding binary systems, Monats. Chem. 91 (1960) 738–740.
[89] I. Dimov, D. Nenov, N. Gidikova, A. Mosheva, Determination of the activity of zinc in liquid manganese and iron alloys, Arch. Eisenhuett. 48 (1977) 209–210.
[90] E. Schmid, G. Siebel, Determination of solid solubility of Mn in Mg by X-ray analysis, Metallwirtschaft 10 (1931) 923–925.
[91] J. Grogan, J. Haughton, Alloys of magnesium. Part XIV. The constitution of the magnesium rich alloys of magnesium and manganese, J. Inst. Met. 69 (1943) 241–248.
[92] N. Tiner, The solubility of manganese in liquid magnesium, Trans. Met. Soc. AIME 161 (1945) 351–359.
[93] G. Siebel, The solubility of iron, manganese and zirconium in magnesium alloys, Z. Metallkd. 39 (1948) 22–27.
[94] A. Schneider, H. Stobbe-Scholder, The structure and technical preparation of corrosion–resistant magnesium–manganese alloys, Metallurgy 4 (9/10) (1950) 178–183.
[95] D. Petrov, M. Mirgalovskaya, I. Strelnikova, E. Komova, The constitution diagram for the magnesium–manganese system, Trans. Inst. Met. 1 (1958) 142–143.
[96] M.V. Chukhov, On the solubility of Mn in liquid Mg. Legkie Splaavy, Akad. Nauk SSSR, Inst. Met. A.A. Baikova 1 (1958) 302–305.
[97] M. Drits, Z. Sviderskaya, L. Rokhlin, Solid solubility of Mn in Mg, Izv. Nauka (1964) 272–278.
[98] Pisch A., Antion C., Tassin C., Baillet F., Gröbner J., Schmid-Fetzer R. Phase Equilibria, Microstructure and Properties of Novel Mg–Mn–Y Alloys in Magnesium Alloys and their Applications, Kainer, K.U. (Ed.), pp. 98–102.
[99] J.L. Haughton, T.H. Schofield, Alloys of magnesium. Part V.—The constitution of the magnesium rich alloys of magnesium and cerium, J. Inst. Met. 60 (1937) 339–344. (Equi Diagram; Experimental).
[100] Rokhlin LL. Solid solubility of neodymium and cerium in solid state magnesium. Izv. Akad. Nauh. SSSR, Otd. Tekh. Nauk, Met. Toplivo, (2), 126–130 (1962) in Russian; TR: Russ. Met. Fuels 1962; 2:98–100. (Equi Diagram; Experimental).
[101] M.E. Drits, Z.A. Sviderskaya, L.L. Rokhlin, The phase diagram of Mg–Ce in the Mg-rich region., Met. Metalloved.Fiz. Khim. Metody, Issled 12 (1963) 143–151 , in Russian. (Equi Diagram; Experimental).
[102] D.H. Wood, E.M. Cramer, Phase relations in the magnesium rich portion of the cerium–magnesium system, J. Less-Common Met. 9 (1965) 321–337. (Equi Diagram, Crys Structure; Experimental).
[103] L.L. Rokhlin, NR. Bochvar, The Mg–La–Ce constitution diagram., Izv. Akad Nauh. SSSR. Met. 2 (1972) 193–197, in Russian; TR: Russ. Metall. 1972; 2:140-3. (Equi Diagram; Experimental).
[104] Q.C. Johnson, G.S. Smith, D.H. Wood, E.M. Cramer, A new structure in the magnesium-rich region of the cerium–magnesium system, Nature 201 (1964) 600. (Equi Diagram, Crys Structure: Experimental).
[105] R. Vogel, On the cerium–magnesium alloys, Z. Anorg. Chem. 91 (1915) 277–298, in German. (Equi Diagram; Experimental).
[106] R. Vogel, T. Heumann, Determination of Ce–Mg and La–Mg systems, Z. Metallkd. 38 (1947) 1–8 , in German. (Equi Diagram, Crys Structure; Experimental;#).
[107] R.R. Joseph, K.A. Gschneidner Jr., Solid solubility of magnesium in some lanthanide metals, Trans. Metall. Sac. AIME 233 (1965) 2063–2069. (Equi Diagram; Experimental).
[108] R.L. Crosby, K.A. Fowler, Studies of magnesium alloys for use at moderate temperatures., U.S. Bur. Mines, Rep. Invest. 6078 (1962) 1–28. (Equi Diagram; Experimental).
[109] Weibke F., Schmidt W. On the solubility of lanthanides in Al, Mg and homogeneous alloys of Mg and Al Z. Electrochem.1940;46:357-364. in German, (Equi Diagram; Experimental).
[110] K. Nagarajan, F. Sommer, Calorimetric investigations of Ce–Mg liquid alloys, J. Less-Common Met. 142 (1988) 319–328.
[111] J.E. Pahlman, J.F. Smith, Thermodynamic of formation of compounds in the Ce–Mg, Nd–Mg, Gd–Mg, Dy–Mg, Er–Mg and Lu–Mg binary systems in the temperature range 650° to 930°K, Metall. Trans 3 (1972) 2423–2432.
[112] A. Palenzona, S. Cirafici, The Ce–Mn (cerium–manganese) system, J. Phase Equilib. 17 (1996) 53–56.
[113] I.V. Nikolaenko, V.V. Nosova, Heats of mixing of manganese with lanthanum, cerium, and praseodymium, Rasplavy 1 (1993) 76–79, in Russian.